Dalton Transactions

ROYAL SOCIETY OF CHEMISTRY

PAPER

View Article Online
View Journal | View Issue

Cite this: *Dalton Trans.*, 2024, **53**, 1551

Hyphenation of lipophilic ruthenium(II)-diphosphine core with 5-fluorouracil: an effective metallodrug against glioblastoma brain cancer cells†

Abhijit Saha,[a] Indranil Mondal,‡[b] Anuj Kumari,‡[b] Avinash Kumar Sonkar,[a] Ramranjan Mishra,[a] Ritu Kulshreshtha[b] and Ashis K. Patra*[a]

Glioblastoma multiforme (GBM) is the most common highly aggressive malignant brain tumor, with a very limited chance for survival post-diagnosis and post-treatment. Despite significant advancement in GBM genomics implicated in molecularly targeted chemotherapies, the prognosis remains poor and requires new drug discovery approaches. We used fluoropyrimidine 5-fluorouracil (**5-FU**), an antimetabolite anticancer drug conjugated or 'caged' within a lipophilic Ru(II)-diphosphine (dppe) core formulated as $[Ru^{II}(dppe)_2(5\text{-}FU)]PF_6$ (**Ru-DPPE-5FU**), where dppe = 1,2-bis(diphenylphosphino)ethane, and evaluated its *in vitro* cytotoxicity in depth with aggressive GBM cells (LN229). The hydrophilic nature of **5-FU** limits its passage through the blood–brain barrier (BBB), which prevents its effective accumulation and efficacy for GBM tumors. Herein, we attempted to modulate the lipophilicity of **5-FU** by inserting it within a well-designed lipophilic $\{Ru(dppe)_2\}$-core with anticipated higher efficiency towards GBM. The physicochemical properties of $[Ru^{II}(dppe)_2(5\text{-}FU)]PF_6$ (**Ru-DPPE-5FU**) were studied using various spectroscopic and analytical techniques. The molecular structure was determined using X-ray crystallography, showing a distorted $\{RuP_4NO\}$ octahedral geometry with bidentate (N, O) binding of **5-FU** and its aromatization in the Ru(II)-bound form. The ^{31}P-NMR spectra of **Ru-DPPE-5FU** showed four closely spaced distinct ^{31}P-signals, indicating four unique chemical environments around P, and the strong coupling constants between them make it a second-order spectrum. The Ru^{II}/Ru^{III} redox potential in **Ru-DPPE-5FU** shifted by ~0.91 V towards the anodic region as compared to its precursor complex *cis*-$[Ru(dppe)_2Cl_2]$ (**Ru-DPPE-Cl**). DFT-based theoretical calculations have been performed to correlate the experimental electronic absorption spectra and redox behaviours of the complexes. The electrostatic potential (ESP) plots indicate the delocalization of the charge density on the O-/F-atom from the 5-FU ligand towards Ru(II) upon its complexation. The antioxidant properties of all the compounds were quantified by a 2,2-diphenyl-1-picrylhydrazyl (DPPH) radical scavenging assay. The hyphenation of the 5-fluorouracil (**5-FU**) ligand to the lipophilic $\{Ru(dppe)_2\}$-core endowed lipophilicity to **Ru-DPPE-5FU** with higher *in vitro* cytotoxicity (IC_{50} = 2.37 μM) against the LN229 GBM cells as compared to the hydrophilic **5-FU**, suggesting efficient cellular uptake. Further biological assays indicated that the complex is highly potent in inhibiting significant proliferation and spheroid formation and restricting the migratory potentials of the GBM cells. Increased caspase 3/7 activity and the presence of apoptotic bodies at the center of 3-D GBM spheroids as revealed by AO/EB dual staining indicated a deeper penetration of the lipophilic complex. The **Ru-DPPE-5FU** complex displayed lower cytotoxicity in HaCaT normal cells (IC_{50} = 7.27 μM) in comparison to LN229 cancer cells with a selectivity index (S.I.) of ≥3. Overall, the synergism and caging of **5-FU** within the hydrophobic $\{Ru(dppe)_2\}$-core improves the pharmacokinetic profile of **Ru-DPPE-5FU** as a potent anticancer agent for glioblastoma.

Received 9th September 2023,
Accepted 29th November 2023

DOI: 10.1039/d3dt02941g

rsc.li/dalton

[a]*Department of Chemistry, Indian Institute of Technology Kanpur, Kanpur 208016, Uttar Pradesh, India. E-mail: akpatra@iitk.ac.in*

[b]*Department of Biochemical Engineering and Biotechnology, Indian Institute of Technology Delhi, Hauz Khas, New Delhi 110016, India*

†Electronic supplementary information (ESI) available: Characterization data (^{1}H, ^{13}C, ^{19}F, ^{31}P-NMR, FT-IR, ESI-MS, CV), X-ray crystallographic details, computational data. CCDC 2294004. For ESI and crystallographic data in CIF or other electronic format see DOI: https://doi.org/10.1039/d3dt02941g

‡Contributed equally.

Introduction

Medicinal inorganic chemists can satisfy their keen intuition and make creative designs for multi-targeted metallodrugs, which are likely to show better efficacy than organic anticancer drugs.[1] Metal complexes offer ample opportunities to modulate their structures, stereochemistry, electronic states, ligand-

exchange kinetics, and multi-targeted delivery ability for chemotherapeutic utilities.[2–4] Ruthenium complexes are capable of exerting anticancer activity *via* exploiting multiple cell death pathways, thereby offering pathways for overcoming the resistance of platins, dose-dependent side effects, improved selectivity, and treatment of a wide range of tumors.[5–8] The advantageous properties of cytotoxic Ru-complexes for chemotherapy include the following: (a) flexible and finely tunable structural diversity influencing the ligand-exchange kinetics, thermodynamic stability, and prolonged circulation lifetime in physiological fluids; (b) the octahedral geometry offers multifaceted modulation of various druggability parameters like attaching multiple ligands for multi-targeted drug designs, and varying lipophilicity and solubility, which are crucial for their cellular uptake and distribution; (c) physiologically accessible Ru^{II}/Ru^{III} oxidation states that allow wider intracellular activation mechanisms. The clinically evaluated Ru-complexes include *trans*-[$Ru^{III}Cl_4$(DMSO)(Im)]ImH (Im = imidazole) (NAMI-A) and *trans*-[$Ru^{III}Cl_4$(DMSO)(Ind)$_2$]IndH (In = indazole) (KP1019/NKP1339) (Na^+ variant), which showed promising antimetastatic and anticancer activities with reduced side-effects.[9]

Glioblastoma multiforme (GBM) is a highly aggressive and deadly tumor of the central nervous system (CNS) that infiltrates and proliferates microscopically throughout the densely woven network of the neuropil.[10] Presently, the standard care of treatment for GBM is surgical resection, followed by radiotherapy, and chemotherapy using temozolomide (TMZ).[11,12] Chemotherapy treatment may be slightly effective but showed significant side effects. Even after these aggressive therapeutics, the rate of survival is only 0.05–4.7% for GBM patients, while without the treatment, the survival is only a few months. Clinical treatment of GBM remains most challenging due to its very aggressive nature and invasive growth.[13,14] The effectiveness of chemotherapy for GBM can be improved by facilitating the ability of chemotherapeutic agents to cross the Blood Brain Barrier (BBB), thus reaching the tumor tissue at therapeutic concentrations, thereby reducing the side effects and enabling sustained therapeutic concentrations of the drugs at the site of the tumor, increasing their half-life, and avoiding rapid clearance.[15] Recently we reported Ru(II)-η^6-*p*-cymene complexes containing Schiff bases derived from 3-aminoquinoline and aromatic hydroxy aldehydes displaying potent anticancer effects in LN229 GBM cells.[16]

5-Fluorouracil (**5-FU**) is a potent antimetabolite drug used for the chemotherapy of GBM using a dual-functionalized liposomal delivery system consisting of the conjugation of the cell-penetrating peptide penetratin to transferrin liposome.[17] Some **5-FU**-appended ligands coordinated to Ru^{II}-(η^6-arene) systems through the pyridyl ring have been previously reported and they showed moderate anticancer activity against the leukemia cell line and exhibited DNA intercalation.[18,19] There is only one report available in the literature with a phosphine-based Ru(II)-complex where the **5-FU** ligand binds directly to the metal center in a bidentate fashion and displays anticancer activity against human colon cancer cells.[20] The hydrophilic nature of **5-FU** limits its ability to cross the BBB, which prevents its accumulation in GBM tumors and limits efficacy. Therefore, in an attempt to improve its efficacy by enhancing its lipophilicity, we strategically and purposefully conjugated 5-fluorouracil (**5-FU**) on a lipophilic ruthenium(II)-1,2-diphenylphosphinoethane anchor, *i.e.*, *cis*-[Ru(dppe)$_2$Cl$_2$] [**Ru-DPPE-Cl**] (Scheme 1).

Herein, we have designed a novel [Ru^{II}(dppe)$_2$(5-FU)]PF_6 (**Ru-DPPE-5FU**) complex to cage **5-FU** within a lipophilic Ru(II)-diphosphine (dppe) core and evaluated the *in vitro* cytotoxicity with aggressive human LN229 GBM cells in detail. The molecular structure and various physicochemical, spectroscopic, and redox properties were thoroughly studied, and DFT-calculations correlated their electronic structures. The antioxidant properties of all the compounds were quantified by the DPPH radical scavenging assay. The enhanced lipophilicity of the **Ru-DPPE-5FU** complex compared to the free hydrophilic **5-FU** drug was achieved. The complex is highly potent at inhibiting

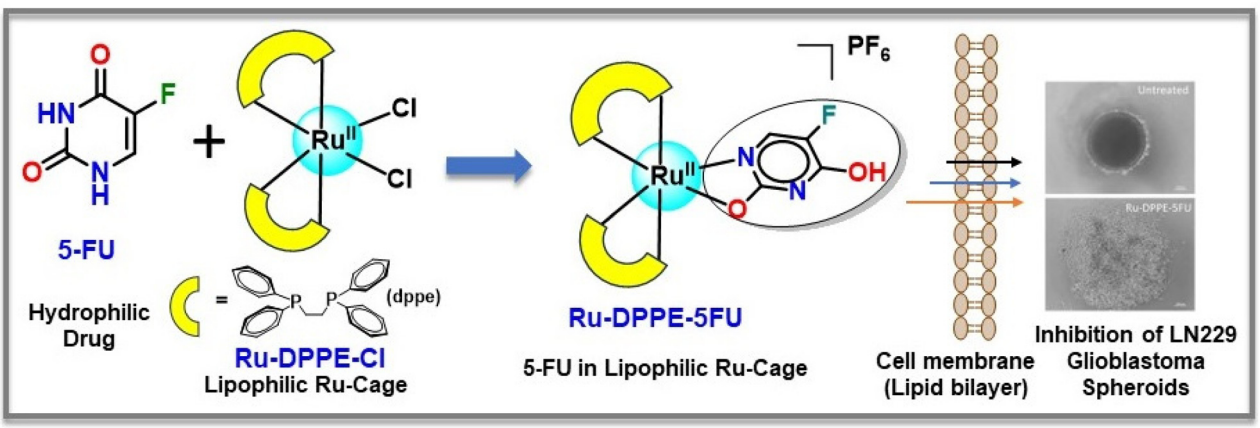

Scheme 1 A typical design strategy for the hyphenation of the lipophilic ruthenium(II)-diphosphine core with hydrophilic 5-fluorouracil (**5-FU**), which is effective against LN229 GBM cells.

proliferation, arresting spheroid formation, and restricting the migratory potentials of the GBM cells. The increased caspase 3/7 activity and apoptotic cells at the core of LN229 spheroids suggest the effective uptake and bioavailability of the lipophilic **Ru-DPPE-5FU** complex. Therefore, the caging of **5-FU** within the {Ru(dppe)$_2$}-core potentially improves the drug-likeness of **Ru-DPPE-5FU** as a potent anticancer agent for glioblastoma.

Results and discussion

Synthesis and characterization

[Ru^{II}(dppe)$_2$(5-FU)]PF$_6$ (**Ru-DPPE-5FU**) was synthesized in good yield (62%) by reacting the precursor *cis*-[Ru^{II}(dppe)$_2$Cl$_2$] (**Ru-DPPE-Cl**) complex with one equiv. of deprotonated 5-fluorouracil (**5-FU**) in methanol : dichloromethane (1 : 1, v/v) under reflux for 12 h in a N_2-atmosphere (Scheme 2). The base-induced deprotonation of **5-FU** resulted in the aromatization of the **5-FU** ring and conversion of the keto group (C=O) to the hydroxy group (–OH) for coordination with Ru(II) as confirmed by the molecular structure from X-ray crystallography (Scheme 2, bottom). The complex was isolated as a faint green-ish-yellow crystalline solid as the PF_6-salt *via* anion exchange using KPF_6.

The **Ru-DPPE-5FU** complex was soluble in MeCN, MeOH, $CHCl_3$, CH_2Cl_2, DMF, DMSO, and insoluble in Et_2O or hydrocarbons, and H_2O. The molecular structure and molecular identity of the **Ru-DPPE-5FU** complex were established by FT-IR, UV-Vis, ^{1}H, ^{13}C, ^{31}P, ^{19}F-NMR, and (^{1}H–^{1}H) COSY NMR spectroscopy and ESI-MS analyses, confirming the structure and purity in the solution. The molecular structure of [Ru^{II}(dppe)$_2$(5-FU)]PF$_6$ in the solid state was determined by single-crystal X-ray diffraction studies.

The FT-IR spectra of the **Ru-DPPE-5FU** complex showed the disappearance of the ν(N–H) peak, which is present in the free **5-FU** ligand, and a new band appeared at around 3441 cm^{-1}, corresponding to ν(O–H) stretching. Similarly, a highly intense peak for ν(C=O) stretching around 1723 cm^{-1} and 1659 cm^{-1} in the free **5-FU** ligand changed to ν(C–O) after complexation and appeared at around 1262 cm^{-1}; the peak observed at 1695 cm^{-1} also corresponds to ν(C=N) in **Ru-DPPE-5FU**. The characteristic vibration of the PF_6^- counter anion assigned to the ν(P–F) was observed at 841 cm^{-1} (Fig. S1, ESI†). The (+)ve mode ESI-MS spectra in MeOH show the molecular ion peak

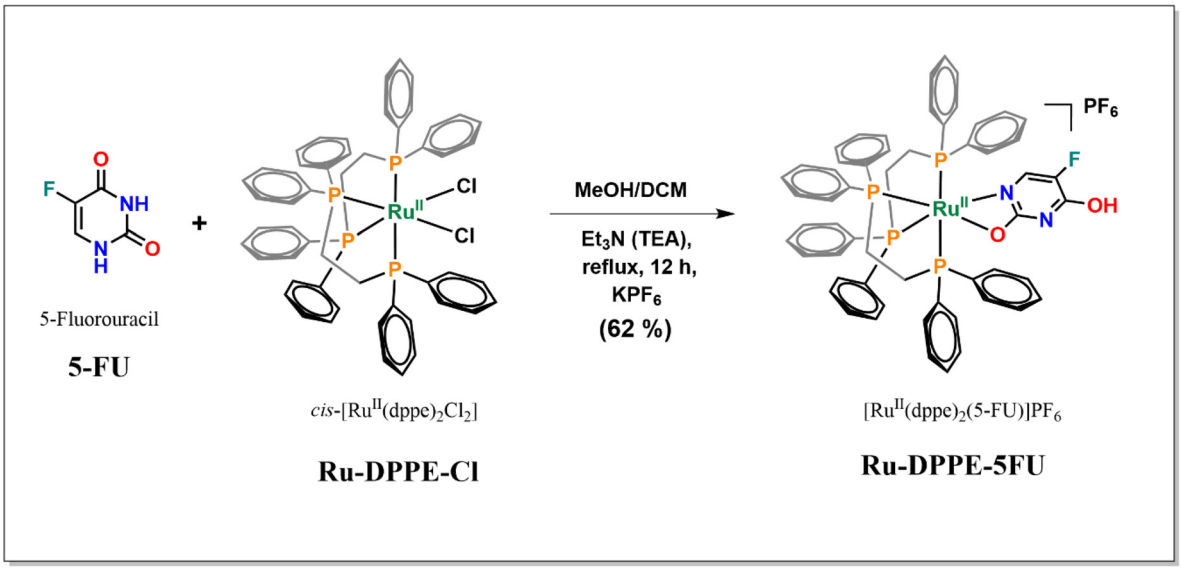

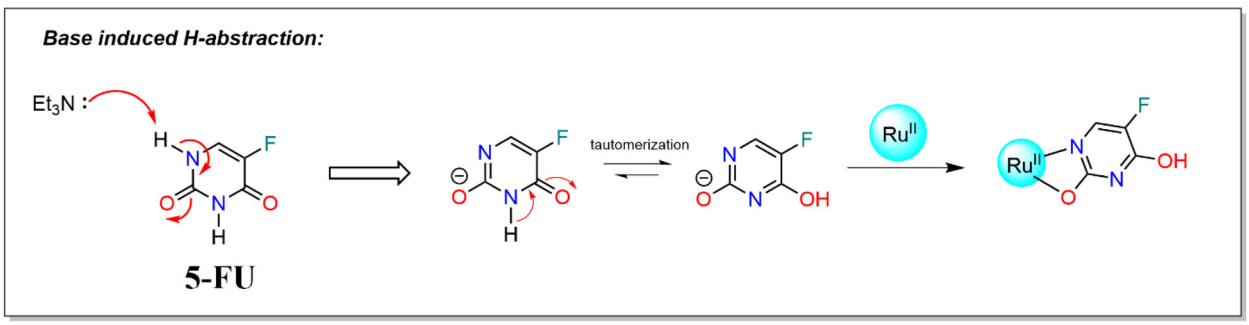

Scheme 2 Synthesis of [Ru^{II}(dppe)$_2$(5-FU)]PF$_6$ (**Ru-DPPE-5FU**) from the reaction of the precursor complex *cis*-[Ru(dppe)$_2$Cl$_2$] (**Ru-DPPE-Cl**) and 5-fluorouracil (**5-FU**). Base-induced proton abstraction from **5-FU** forming its aromatized hydroxylated analogue bound to Ru(II) is shown.

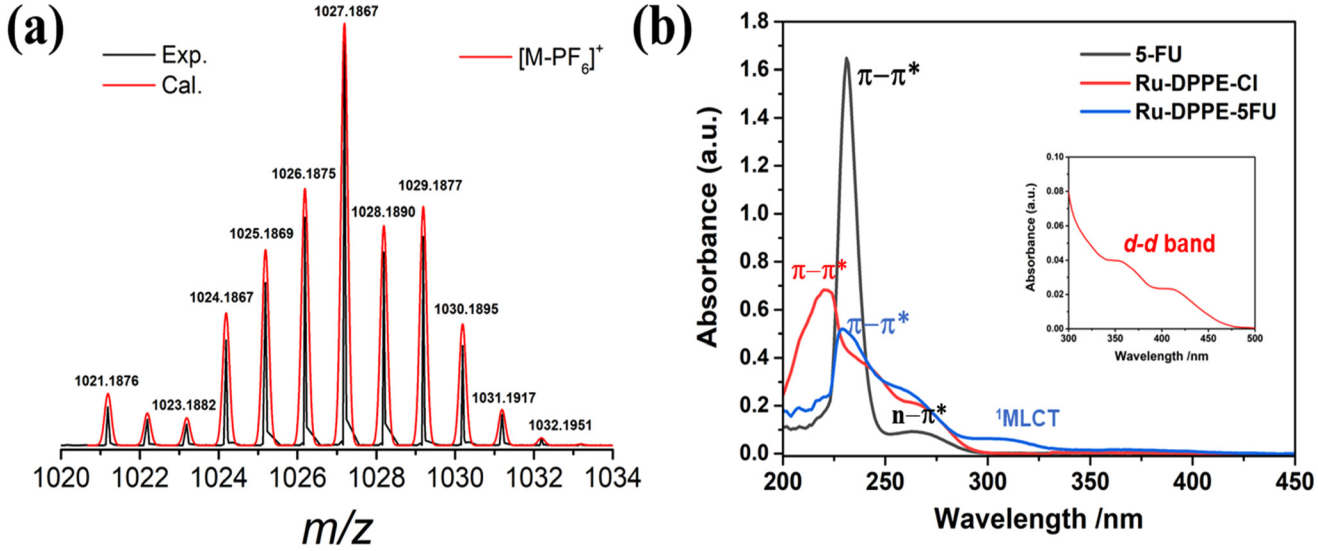

Fig. 1 (a) The isotopic pattern for the $[M - PF_6]^+$ molecular ion peak of **Ru-DPPE-5FU** in methanol by the (+)- ESI-MS technique. (b) UV-visible spectra of **5-FU**, **Ru-DPPE-Cl**, and **Ru-DPPE-5FU** (20 μM) were recorded in dichloromethane. The inset shows the d–d transition band for the *cis*-[Ru(dppe)$_2$Cl$_2$] [**Ru-DPPE-Cl**] complex.

$[M - PF_6]^+$ of the complex cation at m/z = 1027.1867 (calcd m/z = 1027.1850) with a perfectly matching theoretically predicted isotopic distribution pattern confirming its identity in solution (Fig. 1a). The UV-Vis absorption spectra of **5-FU**, **Ru-DPPE-Cl**, and **Ru-DPPE-5FU** were recorded in CH_2Cl_2 solution (Fig. 1b). The **5-FU** ligand showed absorption maxima (λ_{max}) at 229 nm and 263 nm, which were assigned to π–π* and n–π* transitions, respectively. The complex **Ru-DPPE-Cl** showed absorption bands at 221 nm and 261 nm, corresponding to intraligand CT bands, whereas the peaks at 350 nm and 412 nm were assigned as d–d transition bands as previously described by T. J. Meyer and co-workers.[21] The complex [Ru(dppe)$_2$(5-FU)]PF_6 (**Ru-DPPE-5FU**) showed the absorbance bands at 230 nm and 251 nm assigned to the intraligand π–π* transitions, while a peak at 310 nm corresponds to ^{1}MLCT, Ru(dπ) to ligand (π*) transitions.

The solution state speciation and conformation of the complex were studied using multinuclear NMR-spectroscopy. The resolved patterns of resonances in the ^{1}H and ^{13}C NMR spectra were consistent with the low symmetry of the Ru(II) complex (Fig. S2–S4, ESI†). The coordination of 5-FU was confirmed by the presence of ^{1}H- NMR signals at 11.34 and 7.96 ppm, assigned to the protons of the O2–*H* and C4–*H* groups of 5-FU, respectively. This was further confirmed from the ^{19}F-NMR spectra, where the peak at −171 ppm from the free **5-FU** ligand got shifted to −163 ppm upon coordination to the {Ru^{II}(dppe)$_2$} centre in [Ru^{II}(dppe)$_2$(5-FU)](PF$_6$) (Fig. S5, ESI†).

The ^{31}P-NMR chemical shifts ($\Delta\nu$ in Hertz) are closely spaced, meaning that the ^{31}P nuclei have nearly equivalent chemical shifts (not identical), and the coupling constants (J) that connect them are very large, which makes $\Delta\nu/J$ small, and thus the system is said to be strongly coupled; ultimately, the second-order spectrum was observed as shown in Fig. 2a. Here, we also observed the strongly coupled ^{31}P{^{1}H}-NMR spectrum with four distinct signals of doublet-of-doublet of doublet (ddd), found consistent with ABMX pattern spin systems (Fig. 2b); this was also reported earlier by Batista *et al.* in [Ru(dppe)$_2$(N–S)]PF_6 complexes, (where N–S = mercapto ligands).[22] Thus, the four P-atoms in two dppe ligands were chemically and magnetically non-equivalent in [Ru^{II}(dppe)$_2$(5-FU)](PF$_6$) (**Ru-DPPE-5FU**) as also evident from the crystal structure. A characteristic ^{31}P heptet signal around −143 ppm also confirmed the presence of PF_6^- as a counter anion.

Single-crystal X-ray structure

The molecular structure of [Ru^{II}(dppe)$_2$(5-FU)]PF_6 (**Ru-DPPE-5FU**) was determined using single crystal X-ray diffraction studies. The ORTEP view of the complex is shown in Fig. 3. The crystallographic refinement parameters are given in Table S2† and the selected bond distances and angles are listed in Table S3 in the ESI.† The **Ru-DPPE-5FU** complex was crystallized in the monoclinic system with the $P2_1/n$ space group. The [Ru^{II}(dppe)$_2$(5-FU)]PF_6 complex displayed a distorted octahedral geometry with the {RuNOP$_4$}-coordination polyhedron. Herein, the 5-fluorouracil (**5-FU**) ligand was coordinated to Ru(II) through N1 and O1 atoms in a uniquely different bidentate fashion with a delocalized aromatic ring located in the equatorial plane, whereas Batista *et al.* reported a different coordination mode for **5-FU** in [Ru^{II}(5-FU)(PPh$_3$)$_2$(bpy)] through the N2 and O2 atom to Ru(II) in their complex (see Fig. 3).[20] The 3-D perspective view indicates the effective 'caging' of the hydrophilic 5-FU unit within a lipophilic (hydrophobic) pocket consisting of multiple –P(Ph)$_2$ units

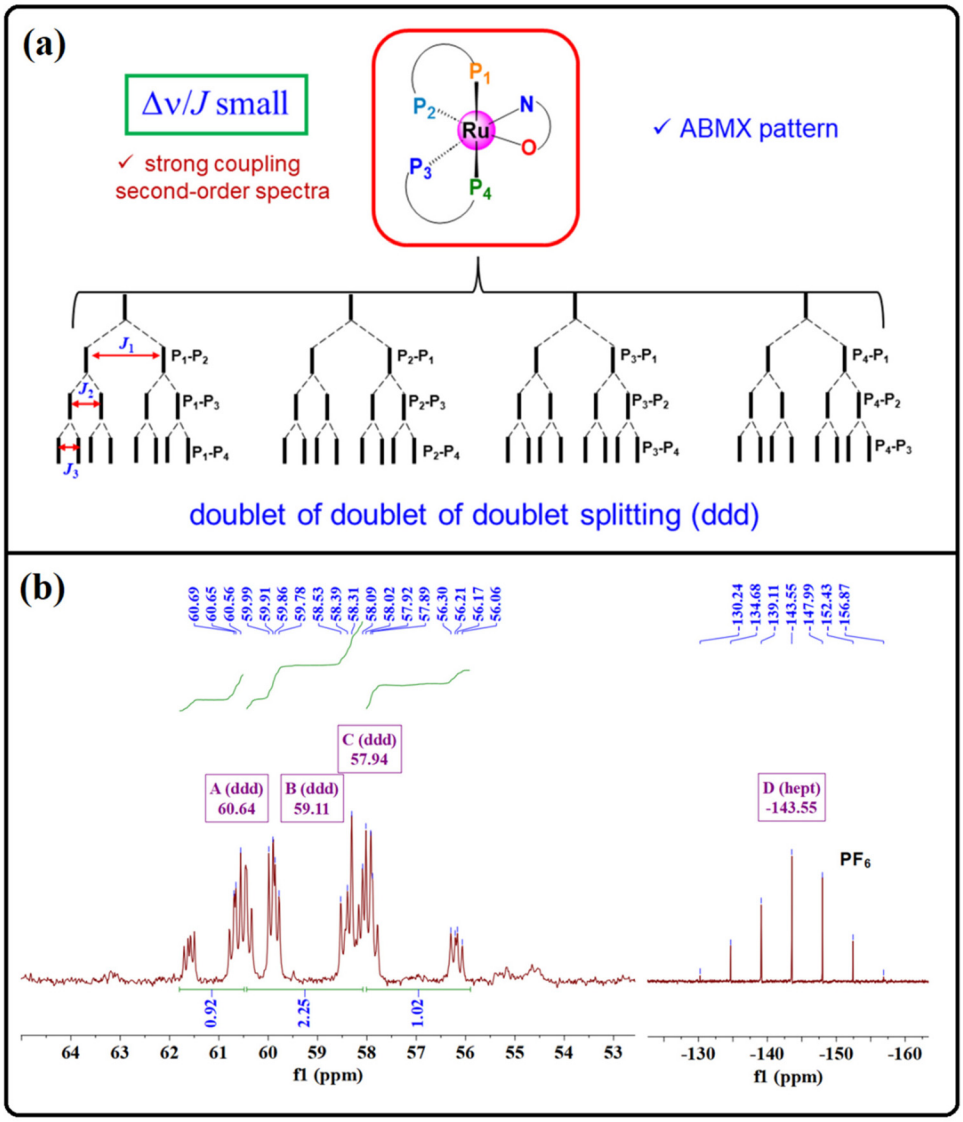

Fig. 2 (a) The second-order splitting pattern of $[Ru^{II}(dppe)_2(5\text{-FU})](PF_6)$ (**Ru-DPPE-5FU**) in the ^{31}P-NMR; (b) the $^{31}P\{^1H\}$-NMR spectrum of **Ru-DPPE-5FU** in DMSO-d_6 at 298 K with reference to 85% H_3PO_4.

of dppe ligands (Fig. S7: space-filled model, ESI†). The coordination of dppe units involves the equatorial-axial binding of the two P-atoms to the Ru(II)-centre, where P1 and P3 atoms occupy the equatorial sites, while the P2 and P4 atoms occupy the axial sites. The Ru1–O1 and Ru1–N1 distances of Ru(II)-5-FU are 2.203 and 2.206 Å, with Ru–P_{ax} bond distances in the range of 2.375–2.396 Å, while Ru–P_{eq} distances were 2.303–2.314 Å for Ru(II)-dppe coordination. Due to the formation of a strained four-membered chelate ring around the Ru-centre, the C1–O1 and C1–N1 bond lengths deviated from the pure single and double bond characters, which were 1.24 Å and 1.36 Å respectively, whereas in the free 5-FU ligand, the bonds were 1.20 Å and 1.40 Å respectively (Table S4, ESI†). This suggests the delocalization of electrons on [O1–C1–N1–Ru1] moiety to gain stability. The C2–O2 and C2–N2 bond lengths of Ru(II)-coordinated 5-FU were ~1.26 Å and ~1.35 Å, respectively, as compared to the free 5-FU ligand (C2–O2: ~1.24 Å, C2–N2: ~1.39 Å).[23] Therefore, upon coordination of 5-FU with the Ru(II) centre, the C2–O2 bond was elongated, while the C2–N2 bond got shortened through the delocalization of electrons to the pyrimidine ring and thereby gaining the aromaticity of the bound 5-FU ligand (Table S4, ESI†). The two nearby axially located mean planes of the phenyl rings originated from P2 and P4 atoms of the dppe and were 3.63 Å and 3.70 Å, respectively, from the equatorially bound 5-FU ligand plane. Such a favourable parallel disposition of aromatic rings resulted in potential intramolecular π···π stacking interactions, thereby sandwiching the bound 5-FU within the lipophilic phenyl groups in **Ru-DPPE-5FU** (Fig. S8a, ESI†). The complex also showed the intra-molecular non-classical H-bonding between C6–H···O1 (distance: 2.145 Å) (Fig. S8b, ESI†).

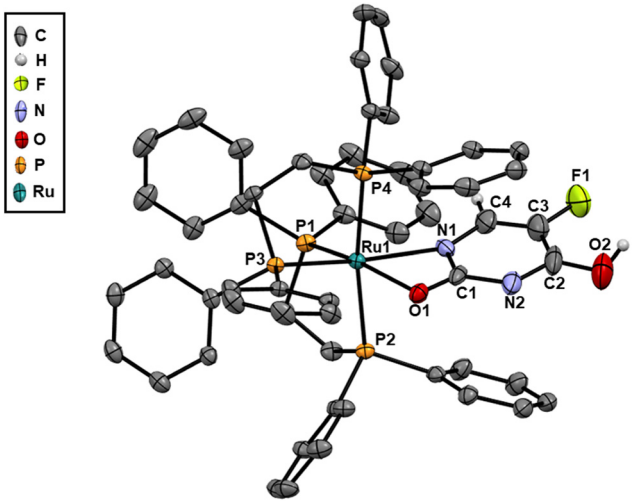

Fig. 3 ORTEP view of the $[Ru(dppe)_2(5\text{-FU})]PF_6$ (**Ru-DPPE-5FU**) ellipsoids at 30% probability with atom numbering of selected atoms. The hydrogen atoms (except 5-FU ring), PF_6^- counter anion, and co-crystallized solvent molecules were omitted for clarity.

Cyclic voltammetry

The cyclic voltammetry experiments for the complexes $[Ru(dppe)_2Cl_2]$ (**Ru-DPPE-Cl**) and $[Ru(dppe)_2(5\text{-FU})]PF_6$ (**Ru-DPPE-5FU**) were carried out in CH_2Cl_2 solutions (Fig. S8 and Table S1†), which presented a quasi-reversible redox process corresponding to one-electron oxidation of Ru^{II}/Ru^{III} couple. Upon scanning towards positive potentials, the half-wave potential ($E_{1/2}$) values shifted from 0.78 V for **Ru-DPPE-Cl** to 1.7 V for **Ru-DPPE-5FU** *vs.* Ag/AgCl (Fig. S8, ESI†). This oxidation behaviour of the ruthenium-centred processes is in agreement with those previously reported for Ru(II)-phosphine complexes.[22,24] The higher anodic peak potential of **Ru-DPPE-5FU** (E_{pa} = 1.74 V) indicates the greater stability of this complex in the Ru(II)-oxidation state as compared to the **Ru-DPPE-Cl** complex (E_{pa} = 0.82 V).

Stability and lipophilicity

The **Ru-DPPE-5FU** complex is soluble and stable in MeOH, DMSO, DMF, $CHCl_3$, and CH_2Cl_2. It is soluble and stable in DMSO/H_2O (1 : 99 v/v) in micromolar concentrations used for biological studies. Therefore, the stability of the $[Ru^{II}(dppe)_2(5\text{-FU})]PF_6$ (**Ru-DPPE-5FU**) complex dissolved in pure DMSO and in a 20% D_2O/DMSO mixture was evaluated by $^{31}P\{^1H\}$-NMR spectroscopy at t = 0, 12, 48, and 72 h (in the case of pure DMSO) and at t = 0, 5, 24, 32, and 42 h (in the case of 20% D_2O/DMSO-d_6 mixture) (Fig. S10 and S11, ESI†). The ^{31}P peaks remained unchanged over this period in the time-dependent $^{31}P\{^1H\}$-NMR spectra, which attested its stability in solution and its structural integrity in DMSO or the D_2O/DMSO solvent mixture during the biological studies.

Lipophilicity is an important property relevant to the ability of the drugs to permeate through biological double-layer cell membranes by passive diffusion. The partition coefficient between octanol and water ($\log P_{o/w}$) is a measure of lipophilicity.[25] The **Ru-DPPE-Cl** and **Ru-DPPE-5FU** complexes showed greater affinity for the organic phase with the distribution coefficients ($\log P_{o/w}$) of 0.79 ± 0.30 and 1.85 ± 0.41, respectively, whereas the free drug **5-FU** showed greater affinity for the aqueous phase with the distribution coefficient ($\log P_{o/w}$) of −0.43 ± 0.08 (Fig. 4). The presence of two 1,2-bis(diphenylphosphino)ethane (**dppe**) ligands in these complexes significantly enhanced the lipophilicity of the complexes. Therefore, the 'caging' of the hydrophilic **5-FU** drug within the lipophilic $\{Ru(dppe)\}_2$-core modulated the overall lipophilic nature and pharmacokinetic profile of the drug. A good correlation between the lipophilicity and the LN229 GBM cell cytotoxicity (IC_{50}) of the complexes was also observed, where the most lipophilic complex **Ru-DPPE-5FU** showed better cytotoxicity with LN229 BGM cells.

Antioxidant activity

Reactive oxygen species (ROS) can promote tumorigenesis by generating DNA mutations or activating pro-oncogenic oxidative-stress-mediated signalling pathways.[26] Thus, antioxidant supplementation has been proposed for the prevention of inflammation-induced cancer *via* cytoprotection and to augment the chemotherapeutic and radiation-based treatments.[27,28] The altered enhanced metabolism in highly proliferative cancer cells tends to have intrinsically higher ROS levels resulting in damage to the surrounding normal cells, hence, the antioxidant ability of the cytotoxic agents is often desirable.[29] Therefore, studying the radical scavenging activity of the present compounds to prevent the carcinogenesis of normal cells will play an important role in evaluating their overall anticancer efficacy.[30] The antioxidant activities of the complexes and the **5-FU** ligand were evaluated by the 2,2-diphenyl-1-picrylhydrazyl (DPPH) radical scavenging assay, initially reported by Blois.[31] The DPPH radical accepts a hydrogen atom or an electron from a radical scavenger, resulting in

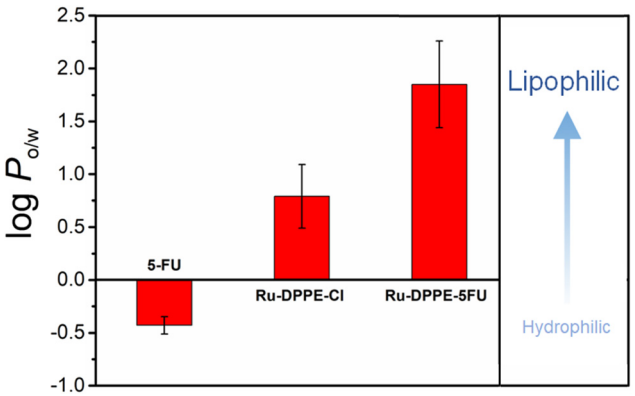

Fig. 4 The lipophilicity index measured as the partition coefficient ($\log P_{o/w}$) for 5-fluorouracil (**5-FU**), *cis*-$[Ru(dppe)_2Cl_2]$ (**Ru-DPPE-Cl**), and $[Ru(dppe)_2(5\text{-FU})]PF_6$ (**Ru-DPPE-5FU**) in a 1 : 1 (v/v) octanol/water mixture, determined from their mean absorbance values by the shake-flask method at 37 °C.

a color change from violet (λ_{max} = 517 nm) to faint yellow (λ_{max} = 340 nm) in solution.[32] Consequently, the percentage of DPPH radical scavenged by the compounds can be monitored by measuring the decreased absorbance at 517 nm in EtOH to give the percentage scavenging activity. The concentration dependence of the scavenging activity (Fig. 5) was used to calculate the EC_{50} values, which are reported in Table 1.

The DPPH assays show that the **Ru-DPPE-Cl** and **Ru-DPPE-5FU** complexes are highly active radical scavengers as compared to the free **5-FU** ligand, with the EC_{50} values of 1 μM, 6 μM, and 481 μM, respectively. We anticipated that the greater scavenging activity of **Ru-DPPE-Cl** and **Ru-DPPE-5FU** could be consistent with the mechanism involving an electron transfer from the Ru(II)-centre to the DPPH radical in the former case since the $E_{1/2}$ (Ru^{III}/Ru^{II}) redox potential is lower; hence a possible H-atom transfer from the phenolic O–H group of the 5-fluorouracil ligand to DPPH could occur in the latter case, as shown in Scheme 3. A similar type of scavenging mechanism was also previously described by Walsby *et al.* for the ferrocene-functionalized Ru(II) complexes, in which they showed, for a piperidine linker, that the DPPH radical was quenched by accepting the ionizable N–H protons; however, the non-piperidine linker-based complexes quenched the DPPH radical by giving one electron from the metal centre itself, since those complexes had lower $E_{1/2}$ (Fe^{III}/Fe^{II}) redox potentials.[33]

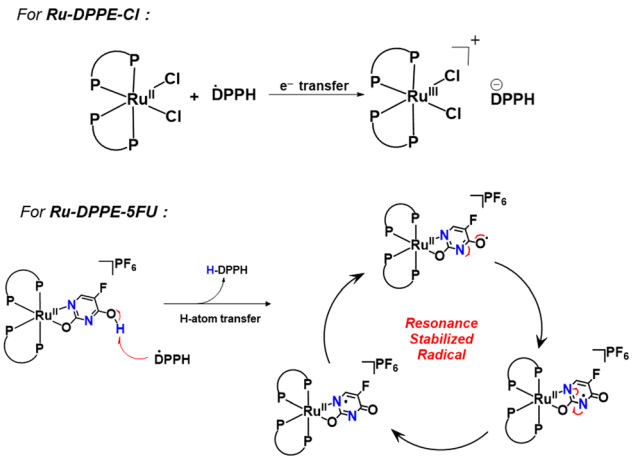

Scheme 3 Proposed mechanism for DPPH radical scavenging pathways in *cis*-$[Ru(dppe)_2Cl_2]$ (**Ru-DPPE-Cl**), and $[Ru(dppe)_2(5\text{-FU})]PF_6$ (**Ru-DPPE-5FU**) related to their antioxidant activities.

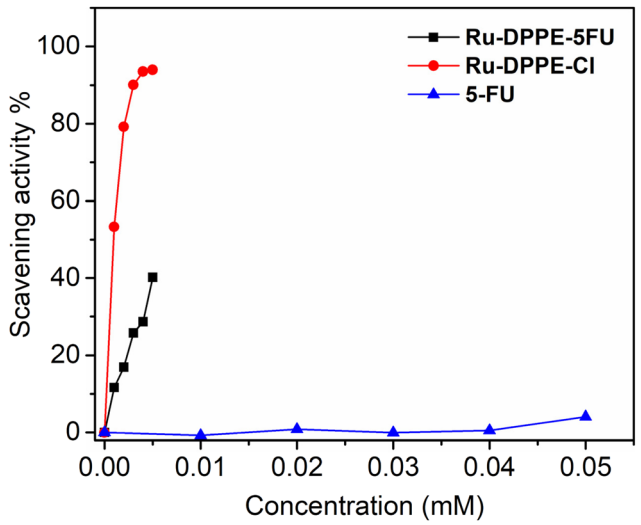

Fig. 5 DPPH radical scavenging assays for **5-FU** (blue), **Ru-DPPE-Cl** (red), and **Ru-DPPE-5FU** (black) with 0.1 mM DPPH in ethanol obtained from UV-visible spectroscopic measurements.

Table 1 The trends in selected physicochemical properties of **5-FU**, **Ru-DPPE-Cl**, and **Ru-DPPE-5FU** relevant to their biological activities

Compounds	$E_{1/2}$ [a] (V *vs.* Ag/AgCl) $E_{1/2}$ (V) (Ru^{III}/Ru^{II})	Lipophilicity[b] $\log P_{o/w}$	Antioxidant activity[c] (EC_{50}) EC_{50} (μM)	Cytotoxicity (IC_{50}) for LN229 GBM cell[d] IC_{50} (μM)
5-FU	—	−0.43 ± 0.08	481	>40
Ru-DPPE-Cl	0.78	0.79 ± 0.30	1	7.368
Ru-DPPE-5FU	1.69	1.85 ± 0.41	6	2.386

[a] Ru^{III}/Ru^{II} reduction potential ($E_{1/2}$ in V) *vs.* Ag/AgCl determined by CV in CH_2Cl_2. [b] Lipophilicity values in terms of partition coefficient $\log P_{o/w}$ in a 1 : 1 (v/v) octanol/water mixture at 37 °C. [c] Antioxidant activity in ethanol in terms of EC_{50} values from DPPH assay. [d] IC_{50} values (μM) for cytotoxicity against LN229 GBM cells measured by MTT assay.

Theoretical studies

The frontier molecular orbitals of **5-FU**, **Ru-DPPE-Cl**, and **Ru-DPPE-5FU** were optimized using density functional theory (DFT) calculations with the B3LYP level 6-31G** basis set for the ligand and SDD basis set for Ru(II) in the studied complexes using the Gaussian 09 program.[34] As illustrated in Fig. 6, the electron density at the HOMO and LUMO of **5-FU** occupied the fluoro-substituted uracil group, whereas the electron density of the HOMO in **Ru-DPPE-Cl**, and **Ru-DPPE-5FU** complexes were mainly localized over the Ru(II)-center while their LUMOs were distributed on the 1,2-bis(diphenylphosphino)ethane (dppe) moiety and the fluoro-substituted uracil group, respectively. The energy gaps between the HOMO and LUMO of **5-FU**, **Ru-DPPE-Cl**, and **Ru-DPPE-5FU** were found to be 5.638 eV, 4.198 eV, and 4.146 eV, respectively, which demonstrate that upon the coordination of the **5-FU** ligand to the $\{Ru^{II}(dppe)_2\}$ core, the energy gap effectively decreased and thereby stabilized the systems. The energy of the HOMO in **Ru-DPPE-5FU** was −6.170 eV, as compared to the HOMO of **Ru-DPPE-Cl** (−5.453 eV), reflecting that the HOMO of **Ru-DPPE-5FU** is energetically more stabilized. In both complexes, the HOMOs are metal-centered so the removal of one electron from ruthenium, *i.e.*, the process of $Ru^{II} \rightarrow Ru^{III}$ oxidation, will be sluggish in the case of **Ru-DPPE-5FU**, which is also evident from the higher anodic peak potential (Ru^{II}/Ru^{III} couple) in the cyclic voltammetry studies.

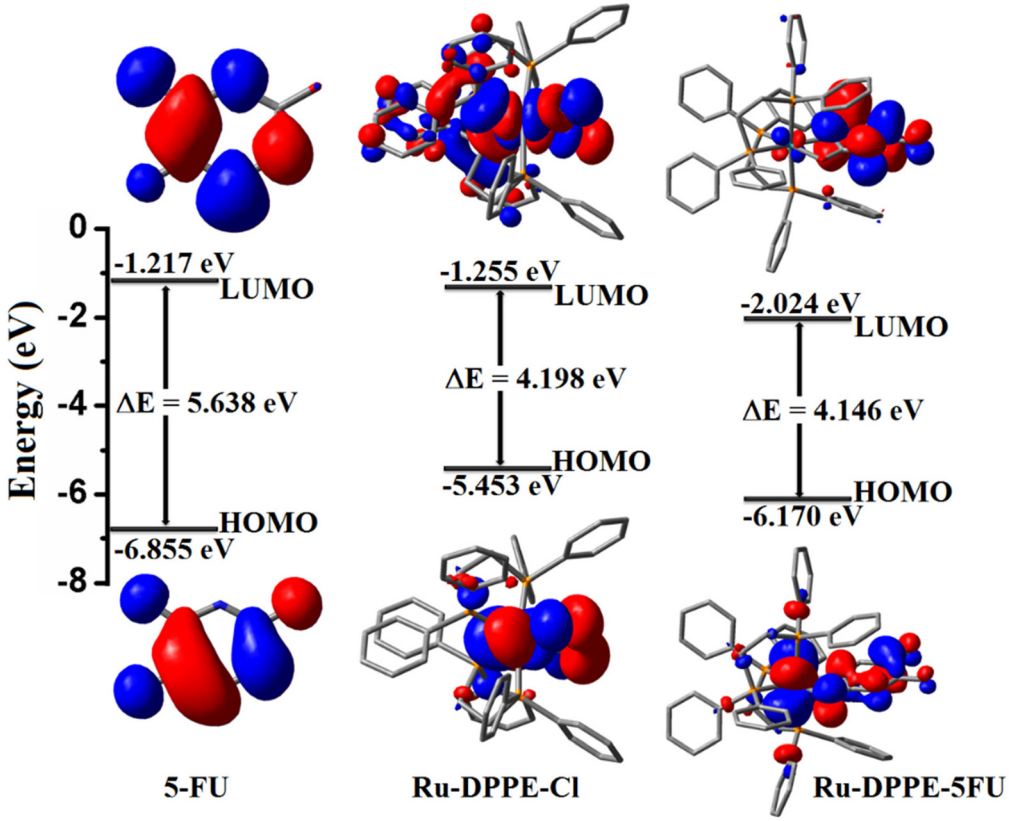

Fig. 6 The energy level diagrams of **5-FU**, **Ru-DPPE-Cl**, and **Ru-DPPE-5FU** calculated at the B3LYP functional level using the 6-31G** and SDD basis sets for the organic ligands and ruthenium, respectively, using the Gaussian 09 program.

To correlate the experimental UV-Vis data, TD-DFT calculations were performed using the B3LYP functional using the 6-31G** and SDD basis sets.[35] The ground state optimized geometries were used for TD-DFT calculations,[36] as well as for the corresponding electronic transitions in CH_2Cl_2. The experimental and theoretical UV-Vis spectra are shown in Fig. 7. The calculated and experimental UV–Vis spectral data together with their assignments are presented in Table S5, ESI.† The TD-DFT results showed that **5-FU** exhibited a major absorbance band at λ_{max} = 249 nm with an oscillator strength of 0.1567. In the case of **Ru-DPPE-Cl**, it exhibited two major absorbance bands at 248 nm and 265 nm with oscillator strengths of 0.0624 and 0.0751 respectively, and two low-intensity bands at 328 nm and 403 nm with the same oscillator strengths of 0.0018. The **Ru-DPPE-5FU** complex exhibited three major absorbance bands with oscillator strengths of 0.0720, 0.1087, and 0.0751, respectively. Overall, from the TD-DFT studies, both experimental and calculated absorbance bands are well-matched with their respective electronic transitions.

The distribution of the electronic charge density can be visualized by mapping the changes in the electrostatic potential (ESP) over the total electron density.[37] The different colors in ESP plots, represent different values of electronic potential. The red color indicates electron-rich regions, while the blue color indicates electron-deficient regions. The ESP plots of **5-FU**, **Ru-DPPE-Cl** and **Ru-DPPE-5FU** are displayed in Fig. 8. The ESP plots clearly indicate greater charge density on the oxygen and fluorine atoms in free **5-FU**, which upon complexation with {Ru(II)-dppe} core, got shifted towards Ru(II), which was also experimentally evident from the downfield ^{19}F-NMR shift for the 5-FU ligand in the **Ru-DPPE-5FU** complex.

In vitro cytotoxicity

The *in vitro* cytotoxic effects of 5-fluorouracil (**5-FU**), *cis*-[Ru(dppe)$_2$Cl$_2$] (**Ru-DPPE-Cl**), and [Ru(dppe)$_2$(5-FU)]PF$_6$ (**Ru-DPPE-5FU**) were evaluated by the MTT cell viability assay using LN229 human brain GBM cells. All the compounds were tested at a minimum of seven concentrations (up to 40 μM) for their cytotoxic effects in the LN229 cell line. While the cytotoxicity of **5-FU** was found to be negligible in this concentration range (Fig. 9A), the **Ru-DPPE-Cl** and **Ru-DPPE-5FU** had significant cytotoxic effects on LN229 cells (Fig. 9B and C). From the dose–response curves, it was observed that **Ru-DPPE-5FU** had significantly higher cytotoxicity as compared to **Ru-DPPE-Cl**, as evident from their IC_{50} values (IC_{50} **Ru-DPPE-Cl** = 7.37 μM, **Ru-DPPE-5FU** = 2.38 μM) (Fig. 9F and G). The phase contrast photomicrographs of LN229 cells treated with 1 μM of both compounds augment this trend. A considerably lower number of viable cells were visible in the **Ru-DPPE-5FU**-treated cells as compared to **Ru-DPPE-Cl** (Fig. 9E). The enhanced cytotoxic

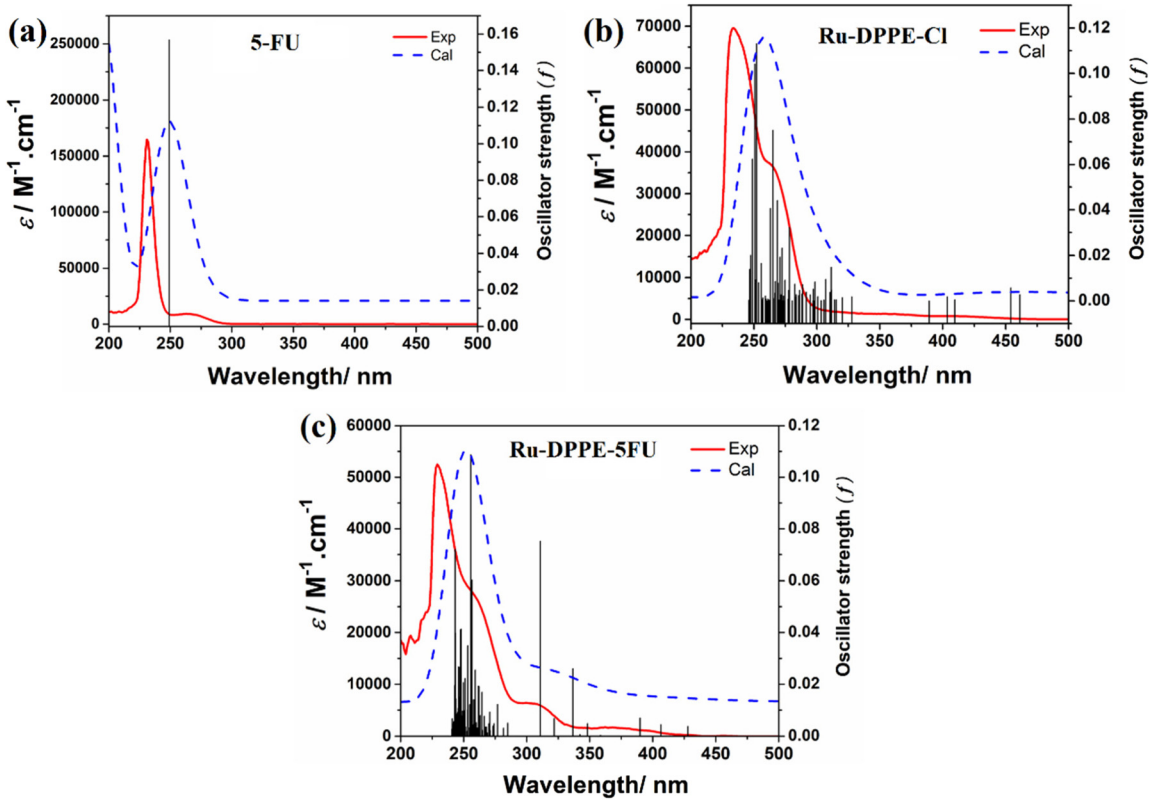

Fig. 7 Experimental and theoretically calculated UV-Vis spectra of (a) **5-FU**, (b) **Ru-DPPE-Cl**, and (c) **Ru-DPPE-5FU** in dichloromethane, and calculated from the TD-DFT calculations at the B3LYP level using the 6-31G** and SDD basis sets.

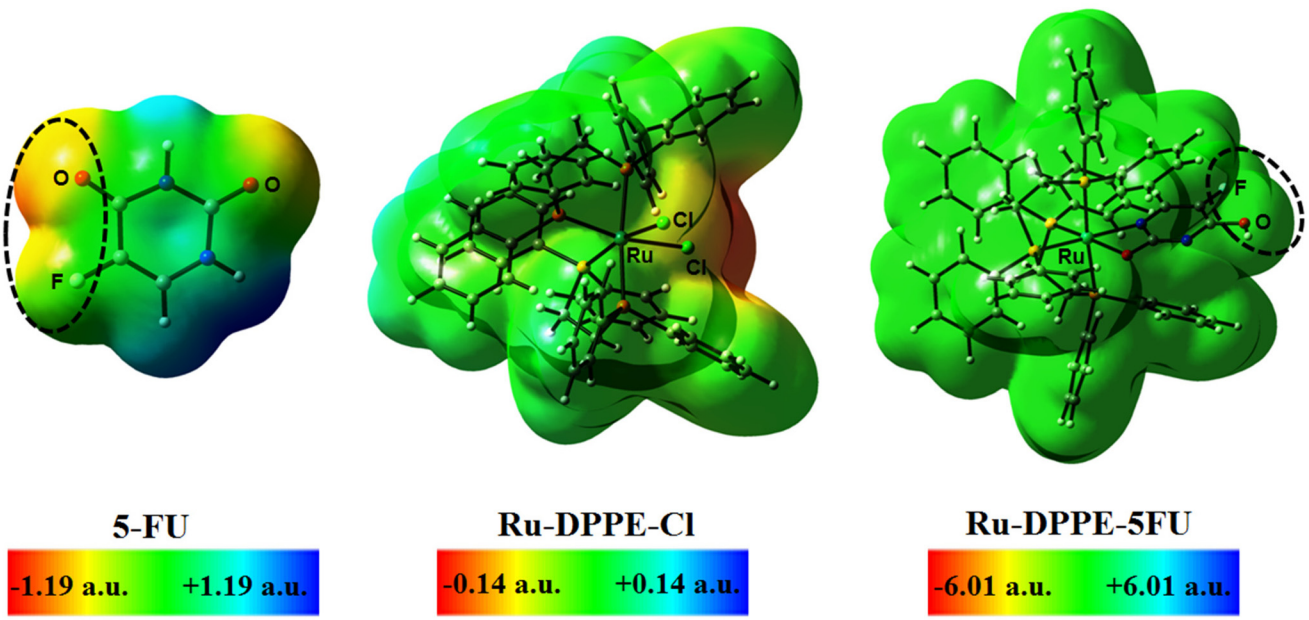

Fig. 8 Molecular electrostatic potential (ESP) mapped on the isodensity surface for (a) **5-FU**, (b) **Ru-DPPE-Cl** and (c) **Ru-DPPE-5FU** in their ground states within the range of −1.19 a.u. (red) to +1.19 a.u. (blue) for **5-FU**, −0.14 a.u. (red) to +0.14e a.u. for **Ru-DPPE-Cl**, and −6.01 a.u. (red) to +6.01 a.u. (blue) for **Ru-DPPE-5FU**, respectively. The change in the electron density in the regions over O and F atoms in free **5-FU** and **Ru-DPPE-5FU** are highlighted.

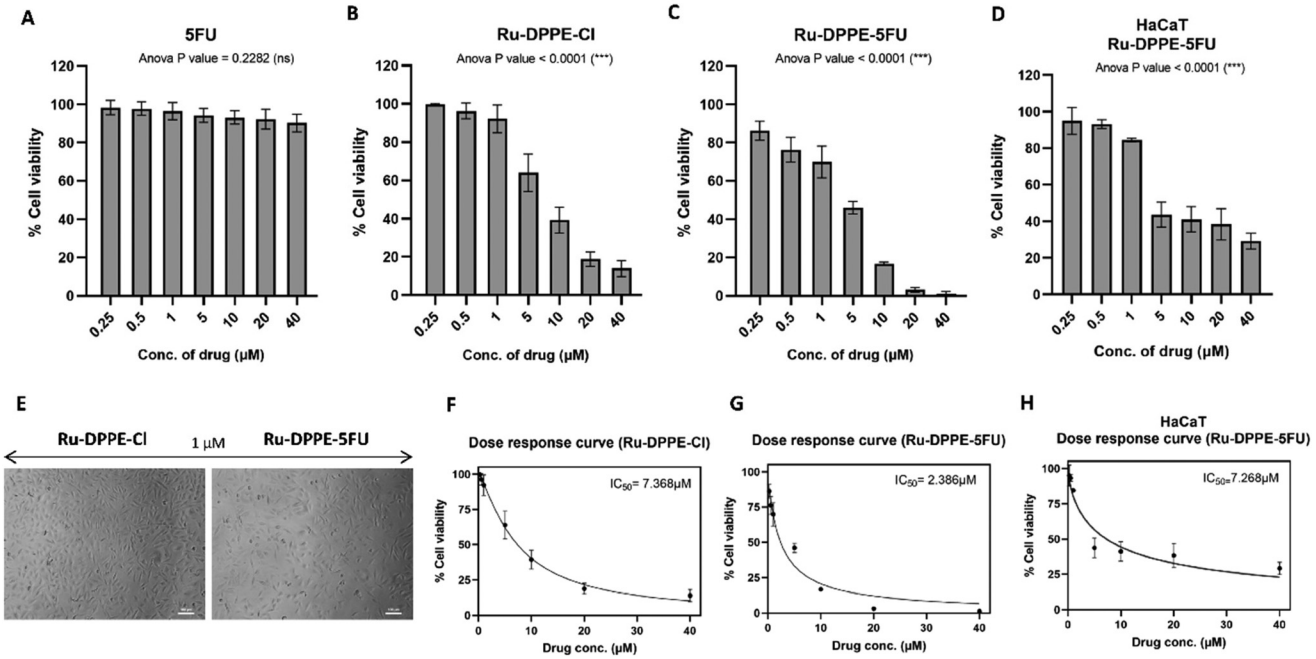

Fig. 9 Cytotoxicity data: %Viability of LN229 cells upon treatment with **5-FU** (A), **Ru-DPPE-Cl** (B), and **Ru-DPPE-5FU** (C). %Viability of HaCaT cells upon treatment with **Ru-DPPE-5FU** (D). Representative photomicrographs of LN229 cells treated with **Ru-DPPE-Cl** and **Ru-DPPE-5FU** compounds at 1 μM concentration (E). determination of IC_{50} values of **Ru-DPPE-Cl** and **Ru-DPPE-5FU** in LN229 cells (F and G). Determination of IC_{50} values of **Ru-DPPE-5FU** in HaCaT normal cells (H).

effects of **Ru-DPPE-5FU** as compared to its parent compound **Ru-DPPE-Cl** is possibly due to the strong synergistic anti-cancer effects of the {Ru(II)(dppe)$_2$}-core and **5-FU**, along with enhanced cellular uptake due to increased lipophilicity as discussed previously. Further, the cytotoxic effects of **Ru-DPPE-5FU** were also checked in the HaCaT cell line as a control/normal cell line to measure the drug selectivity index (S.I.). **Ru-DPPE-5FU** had significantly lower cytotoxic effects on HaCaT cells (IC_{50} **Ru-DPPE-5FU** = 7.27 μM) (Fig. 9H) in comparison to the LN229 cells. The selectivity index (S.I.) for **Ru-DPPE-5FU** was 3.04, which represents the greater selectivity and potency of **Ru-DPPE-5FU** towards brain cancer cells.

Inhibition of cellular proliferation

Uncontrolled growth and rapid cellular proliferation are crucial hallmarks of tumour progression. To check its efficacy as a potent anti-cancer agent, **Ru-DPPE-5FU** was tested for its anti-proliferative effects in LN229 cells. Its impact on cellular proliferation was investigated by its long-term incubation (for up to 3 days) with the GBM cells at 1 μM concentration. A concentration lower than the IC_{50} value was chosen for the treatment to avoid imminent cell death and observe its efficacy at lower concentrations over a prolonged time. The cell viability after regular intervals was determined using an MTT assay. It was observed that **Ru-DPPE-5FU** treatment significantly inhibited the proliferation of LN229 cells on days 2 and 3 (Fig. 10A). Our study proved that **Ru-DPPE-5FU** is an efficient anti-proliferative drug for LN229 GBM cells.

The effect on 3D-spheroid formation ability

The ability of tumour cells to come together to form a spheroid in an anchorage-independent manner and increase in size is a measure of its aggressiveness, as well as proliferative capability. When the effect of **Ru-DPPE-5FU** on the 3D-spheroid forming ability of LN229 cells was investigated, the untreated control group of cells was able to generate spheroids, however, the cells that received **Ru-DPPE-5FU** treatment did not form any spheroids (Fig. 10B). This showed the strong and highly desirable anti-cancer effects of [Ru(dppe)$_2$(5-FU)]PF_6 (**Ru-DPPE-5FU**), which successfully reduced the aggressiveness of LN229 cells and prevented them from forming 3D-spheroids.

The effect on cellular migration *via* the wound healing assay

A high cellular migration is an important cancer hallmark, which plays a key role in cancer progression, metastasis, and tumour development. To evaluate the impact of **Ru-DPPE-5FU** on GBM cell migration, the *in vitro* scratch assay/wound healing assay was performed in which the relative gap closure rate of LN229 cells after scratching was measured. It was observed that the GBM cells that were treated with the **Ru-DPPE-5FU** had significantly lower migratory potential than the untreated control group of cells. We observed approximately 70% reduction of cellular migration in the treated group as compared to the control group, reflecting a very effective inhibition of the migratory potential of the highly aggressive GBM cells (Fig. 11A and B).

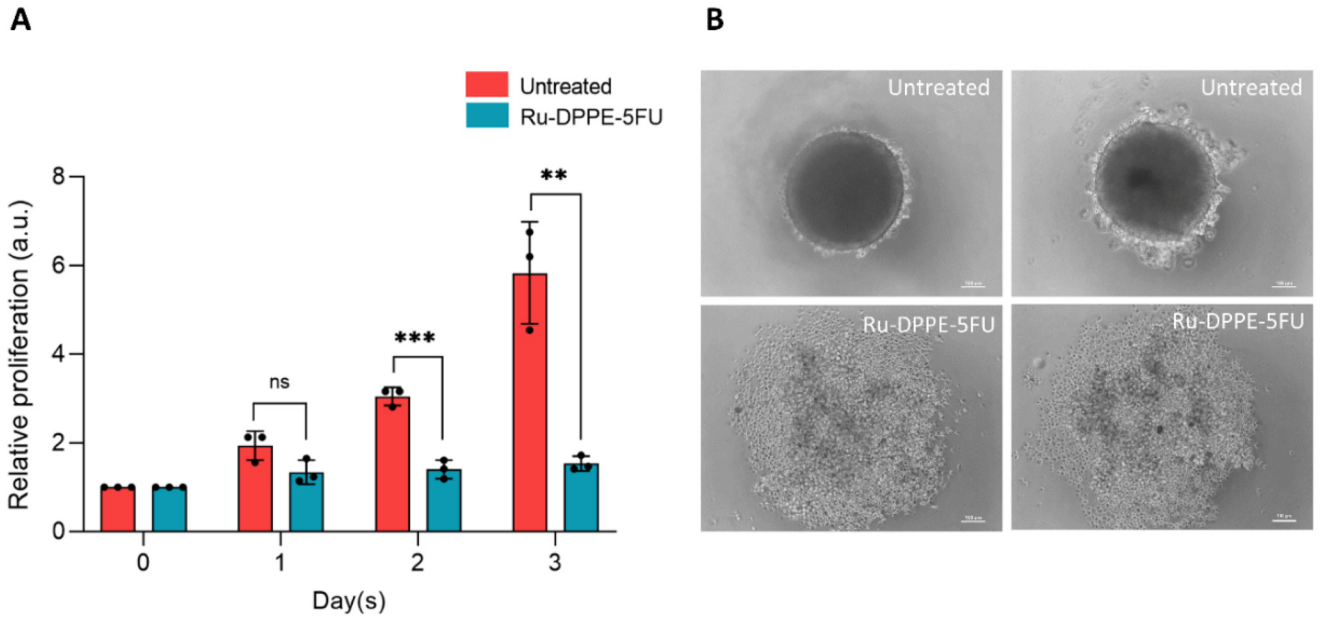

Fig. 10 Anti-proliferative effects of $[Ru(dppe)_2(5\text{-}FU)]PF_6$ (**Ru-DPPE-5FU**): (A) **Ru-DPPE-5FU** complex at 1 μM concentration significantly inhibits cellular proliferation on days 2 and day 3. (B) **Ru-DPPE-5FU** treatment inhibits the 3D-spheroid formation of LN229 cells shown for two spheroids. The experiment was repeated n = 3 times. Statistical significance levels for the experiment: *p > 0.01 and <0.05, **p < 0.01, ***p < 0.001. Error bars represent ± SD.

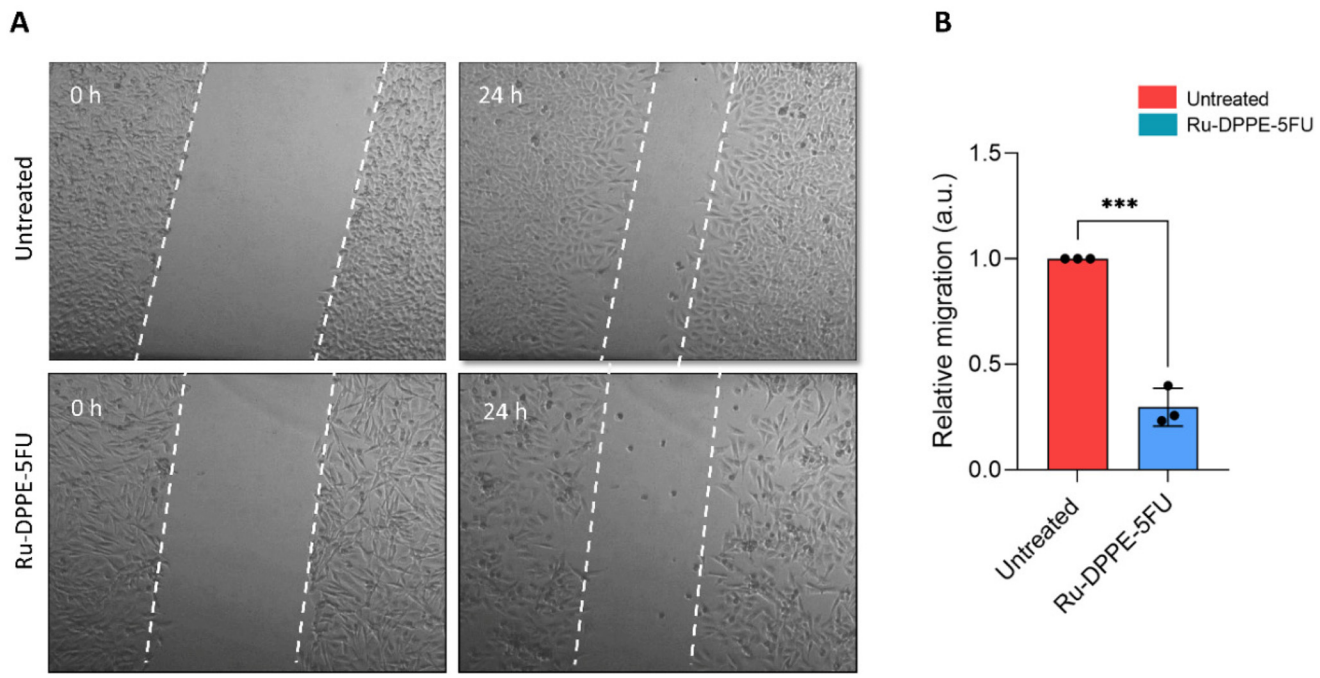

Fig. 11 The inhibition of cellular migration by **Ru-DPPE-5FU**: (A) phase-contrast photomicrograph representing the decreased migration of **Ru-DPPE-5FU**-treated LN229 cells. (B) Quantification of the migratory potential of LN229 cells in the presence or absence of **Ru-DPPE-5FU**, as obtained from (A). The experiment was repeated n = 3 times. *p > 0.01 and <0.05, **p < 0.01, ***p < 0.001. Error bars represent ± SD.

The effects on apoptosis from AO/EB dual staining and caspase activity

Apoptosis is an irreversible mode of programmed cell death and an important hallmark of tumour progression. The effects of **Ru-DPPE-5FU** treatment on the apoptosis of GBM cells were investigated by measuring the activity of two major executioner caspases 3 and 7. It was observed that **Ru-DPPE-5FU**-treated LN229 cells had a mean increase of 38.93% in their caspase 3/7 activity (Fig. 12B). Also, when the cells were stained with acridine orange (AO)/ethi-

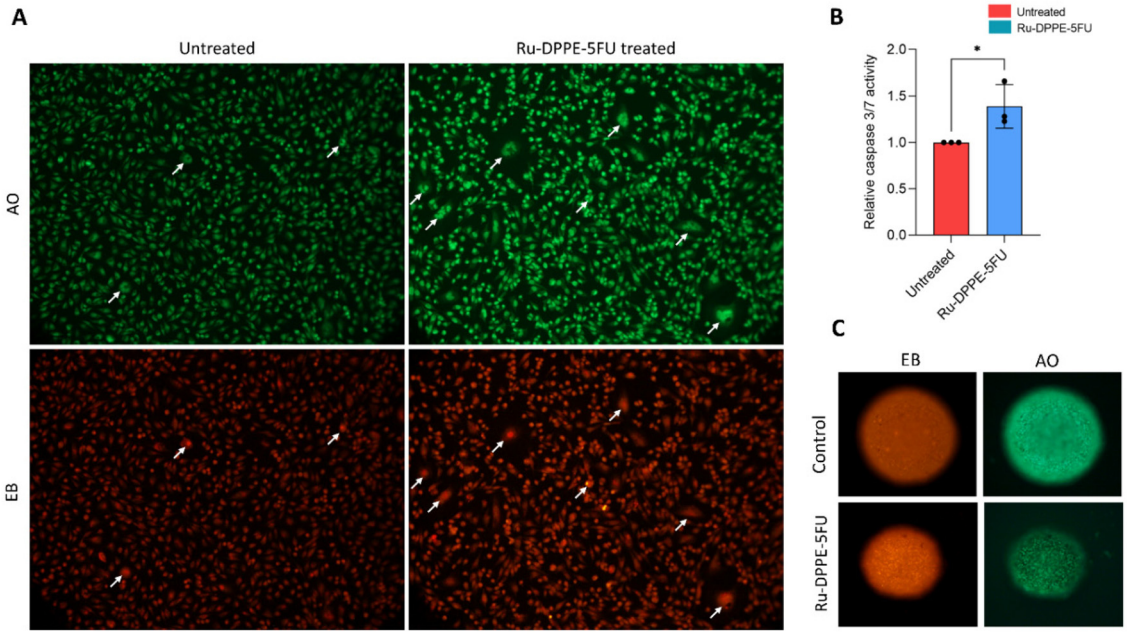

Fig. 12 The $[Ru(dppe)_2(5\text{-FU})]PF_6$ (**Ru-DPPE-5FU**) treatment promotes GBM cells apoptosis: (A) AO/EB dual staining highlights an increased number of apoptotic cells in the **Ru-DPPE-5FU** treatment group. (B) The **Ru-DPPE-5FU** treatment increases the caspase 3/7 activity of GBM cells as compared to untreated cells, the experiment was repeated $n = 3$ times. *$p > 0.01$ and <0.05, **$p < 0.01$, ***$p < 0.001$. Error bars represent ± SD. (C) The AO/EB dual staining in 3D-spheroids of GBM cells shows more apoptotic cells in the **Ru-DPPE-5FU** treatment group. Images were taken at 10× magnification.

dium bromide (EB) dual staining solution, an increase in apoptotic cells was observed in the **Ru-DPPE-5FU**-treated group. Acridine orange is a cell-permeant dye that upon binding to the nucleic acid emits green fluorescence. Therefore, the cells with intact as well as damaged membranes both take up this dye. However, the cells undergoing early apoptosis show bright green dots in their nucleus, suggesting the condensation of chromatin. On the other hand, cells that have lost membrane integrity actively take up EB and show bright orange fluorescence. We observed that the **Ru-DPPE-5FU**-treated cells had a higher number of apoptotic cells as evidenced by the bright green and orange fluorescence in their nucleus (Fig. 12A). Interestingly, we also observed a similar trend in the 3D spheroid models of GBM. When the spheroids were incubated in the presence of **Ru-DPPE-5FU**, the bright orange dots were visible even at the center of the spheroid. This indicated that **Ru-DPPE-5FU** not only triggered the apoptosis of the cells at the leading edge but also the cells at the center of spheroids were affected (Fig. 12C). This is quite an interesting finding as the drug showed remarkable promise for penetrating the boundary of a solid tumor and reaching its center, which is often a great limitation for the treatment of solid tumors and could prevent metastasis due to the migration of unaffected cancer cells.

Conclusions

We have rationally designed a novel Ru(II)-diphosphine (dppe)-based lipophilic cationic complex $[Ru^{II}(dppe)_2(5\text{-FU})]PF_6$ (**Ru-DPPE-5FU**), where we caged a hydrophilic anticancer antimetabolite, 5-fluorouracil (**5-FU**) within the$\{Ru(dppe)_2\}$ core. Here, we attempted to modulate the lipophilicity of **5-FU** by inserting it within a lipophilic $\{Ru(dppe)_2\}$-core in anticipation of greater efficiency towards LN229 GBM cells. The molecular structure of **Ru-DPPE-5FU** was determined by X-ray crystallography, and the physicochemical properties were thoroughly studied using various spectroscopic methods. The experimental results suggest the aromatization of the 5-FU ligand upon coordination to Ru(II). The complex showed $Ru^{II/III}$ or 5-FU ligand-centered redox-mediated efficient antioxidant properties, which were quantified by DPPH assay. The DFT/TD-DFT-based theoretical calculations were performed to correlate the experimental electronic absorption spectra and redox behaviors of the complexes. It is noteworthy that the conjugation of 5-fluorouracil (**5-FU**) to the lipophilic $\{Ru(dppe)_2\}$-core endowed enhanced lipophilicity to **Ru-DPPE-5FU** with greater *in vitro* cytotoxicity against the LN229 GBM cells as compared to the hydrophilic **5-FU**, suggesting efficient cellular uptake. The biological assays indicate that the **Ru-DPPE-5FU** complex is highly potent in inhibiting rapid proliferation, 3-D spheroid formation, and restricting the migratory potential of the LN229 GBM cells, suggesting its effectiveness. It also lowered the migratory potential correlated with tumor progression and metastasis. Increased caspase 3/7 activity and the presence of apoptotic bodies at the center of the 3-D GBM spheroids as revealed by the AO/EB dual staining indicated the deeper penetration of the lipophilic complex and caused apoptotic cell death. Furthermore, the selectivity index (≥3) of **Ru-DPPE-5FU** lies in a moderate range, favoring drug

selectivity towards GBM cells. Overall, this work underscores a new platform and a generalized strategy for fine-tuning the pharmacokinetic profile, lipophilicity, and druggability for developing future Ru(II)-based chemotherapeutic agents.

Experimental

Materials and methods

Reactions and chemicals were handled under a nitrogen or argon atmosphere. Solvents were purchased directly from Thermo Fischer Scientific India Pvt. Ltd and were used without further purification. $RuCl_3{\cdot}xH_2O$, 1,2-bis-(diphenylphosphine) ethane (dppe) ligand, 5-fluorouracil (**5-FU**) ligands were used as received from Sigma-Aldrich and triethylamine (NEt_3) was purchased from RANKEM Laboratory reagents. The *cis*-$[Ru(dppe)_2Cl_2]$ (**Ru-DPPE-Cl**) complex was used as a precursor for the synthesis of the target complex $[Ru(dppe)_2(5\text{-}FU)]PF_6$ *i.e.*, **Ru-DPPE-5FU**.

Instrumentation

Fourier transform infrared spectra (FTIR) were recorded in KBr pellets on a PerkinElmer 1320 instrument in the range 4000–400 cm^{-1}. ESI-MS mass spectral measurements were obtained on a WATER Q-TOF Premier Mass spectrometer. ^1H, $^{31}P\{^1H\}$-NMR, $^{19}F\{^1H\}$-NMR, $^{13}C\{^1H\}$-NMR, and COSY(^1H–^1H) spectra were recorded with a JEOL ECX-400 FT (400 MHz) and a JEOL ECX-500 FT (500 MHz) instrument at 298 K using chemical shifts, which are reported in relation to 85% H_3PO_4, $CFCl_3$ and DMSO-d_6. The UV-Vis spectra of the complexes were recorded in CH_2Cl_2 on a *JASCO V*-670 spectrophotometer. Electrochemical measurements were performed using a CH Instruments Model CHI610E potentiostat, with a glassy carbon working electrode, an Ag/AgCl reference electrode, and a platinum wire auxiliary electrode, and carried out at room temperature under a N_2 atmosphere. The typical conditions were 0.1 M Bu_4NPF_6 ($TBAPF_6$) as a supporting electrolyte in CH_2Cl_2 solvent. In dichloromethane solvent, the Fc^+/Fc redox potential ($E_{1/2}$) was +0.624 V *vs.* the Ag/AgCl reference electrode in our system.

X-ray crystallography

Single crystals of the complex **Ru-DPPE-5FU** were grown from the slow evaporation of CH_2Cl_2 in the presence of a small amount of DMSO. A single crystal of suitable dimensions was mounted on a glass fibre and used for data collection. All the geometric and intensity data were collected on a Bruker D8 Quest Microfocus X-ray CCD diffractometer equipped with an Oxford Instruments low-temperature attachment, with graphite-monochromatic Mo Kα radiation (λ = 0.7103 Å) at 100 (2) K using the ω-scan technique (width of 0.5° per frame) at a scan speed of 10 s per frame, controlled by the manufacturer's APEX v2012.4-3 software package.[38] Intensity data collected using ω–2θ scan mode were corrected for Lorentz-polarization effects,[39] processed, and integrated with Bruker's SAINT software.[40] Absorption corrections were done using the SADABAS program.[41] All the crystal structures were solved in OLEX2, and models were refined by full-matrix least squares on F^2 using SHELXTL.[42] All non-hydrogen atoms were refined anisotropically. Diagrams and publication material were generated using OLEX2.[43] The ORTEP view of the molecular structure is shown in Fig. 3, and its detailed crystallographic parameters are presented in the ESI.†

Synthesis of *cis*-$[Ru^{II}(dppe)_2Cl_2]$ ([Ru-DPPE-Cl])

cis-$[Ru^{II}Cl_2(dmso)_4]$ (0.25 g, 0.516 mmol) and 1,2-bis-(diphenylphosphino)-ethane (dppe, 0.432 g, 1.084 mmol) were dissolved in CH_2Cl_2 (40 mL) and stirred at 0 °C. After 2 h of stirring, the clear yellow solution was allowed to attain room temperature and concentrated under vacuum to about 3–5 mL, then Et_2O was added. The dark yellow solid obtained was collected by filtration and washed with three 15 mL portions of Et_2O and dried under vacuum. Both the *cis* and *trans*-$[Ru^{II}(dppe)_2Cl_2]$ isomers were formed in this reaction but the *cis*-isomer was the major product. The separation of the *cis*-product from the *trans* was carried out by making a concentrated solution in CH_2Cl_2 and placing a layer of hexane above this; upon cooling, the pure *cis*-$[Ru^{II}(dppe)_2Cl_2]$ isomer crystallized out as previously reported by Morris and co-worker and was characterized accordingly.[44] Yield: 0.415 g (0.42 mmol, 83%). ESI-MS(+)ve (CH_2Cl_2): calc. (m/z) 933.1438; found (m/z) 933.1460 $[M - Cl]^+$ (Fig. S15, ESI†). UV–vis [CH_2Cl_2; λ/nm (ε/M^{-1} cm^{-1})]: 234 (69 510, ILCT), 264 (36 837, ILCT), 354 (1347, d–d transitions), 410 (778, d–d transitions). ^1H-NMR (400 MHz, DMSO-d_6) δ 8.18–8.15 (m, 4H), 7.62 (dt, J = 7.4, 4.2 Hz, 4H), 7.23–7.21 (m, 6H), 7.08–6.91 (m, 10H), 6.79–6.75 (m, 12H), 6.60 (t, J = 8.1 Hz, 4H), 2.54 (s, 8H). $^{13}C\{^1H\}$-NMR (101 MHz, DMSO-d_6) δ 136.04, 133.96, 133.10, 130.87, 130.64, 128.49, 127.98, 127.65, 127.29, 126.59, 126.10, 40.43 [*for obtaining the ^{13}C-NMR spectra, a small amount of $CDCl_3$ was used, showing residual solvent peaks ~δ 78.96–78.30]. $^{31}P\{^1H\}$-NMR (160 MHz, DMSO-d_6) δ 50.85 (t, J = 19.5 Hz, 2P), 38.42 (t, J = 19.5 Hz, 2P) (Fig. S12–S14, ESI†).

Synthesis of $[Ru^{II}(dppe)_2(5\text{-}FU)]PF_6$ ([Ru-DPPE-5FU])

In a 50 mL round-bottom flask, a mixture of *cis*-$[Ru^{II}(dppe)_2Cl_2]$ (**Ru-DPPE-Cl**) (0.20 g, 0.206 mmol) and 1.5 equiv. of 5-fluorouracil (**5-FU**) (0.041 g, 0.315 mmol) with NEt_3 (0.048 mL, 0.336 mmol) as a base were added to 30 mL of 1 : 1 v/v (CH_2Cl_2 : MeOH). The reaction was carried out under reflux at 55 °C for 12 h. Thereafter, the reaction mixture was cooled to room temperature, the solvent volume was reduced to 5 mL, and a saturated aqueous KPF_6 solution was added to it, which gave a faint yellowish precipitate, and then the solid product was washed 3 times with water and diethyl ether to obtain the desired product as a crystalline solid. The compound was then purified by silica gel column chromatography using a mixture of 1% MeOH/DCM as the eluent, the first greenish-yellow fraction gave the pure product. Yield: 0.15 g (0.128 mmol, 62%). ESI-MS(+)ve (MeOH): calc. (m/z) 1027.1850; found (m/z) 1027.1867 $[M - PF_6]^+$ (Fig. 1a, Fig. S6, ESI†). FT-IR (KBr matrix, ν/cm^{-1}): 3441 (O–H, br), 3059 (sp^2 C–H, w), 1695 (C═N, s), 1436 (C–F, s), 1262 (C–O, s), 841 (P–F, sh) [br, broad, sh, sharp, w, weak, s, strong]. UV–vis [CH_2Cl_2; λ/nm (ε/M^{-1} cm^{-1})]: 229

(52 500, ILCT), 260 (26 605; ILCT), 310 (5980, ^{1}MLCT). ^{1}H-NMR (400 MHz, DMSO-d_6) δ 11.34 (O–$H_{5\text{-FU}}$), 8.23–8.07 (m, 1H, dppe Ar–H), 7.94 (t, J = 8.7 Hz, 1H, $H_{5\text{-FU}}$), 7.80–6.91 (m, 34H, dppe Ar–H), 6.70 (d, J = 15.4 Hz, 1H, dppe Ar–H), 6.41 (t, J = 8.9 Hz, 1H, dppe Ar–H), 5.98–5.63 (m, 3H, dppe Ar–H), 2.74–1.58 (m, 8H, dppe –CH_2). ^{13}C{^{1}H}-NMR (101 MHz, DMSO-d_6) δ 159.46, 154.83, 135.77–128.14, 17.42–15.48. ^{31}P{^{1}H}-NMR (160 MHz, DMSO-d_6) δ 60.64 (ddd, J = 216.5, 30.9, 21.9 Hz, 1P), 59.11 (ddd, J = 274.6, 30.9, 17.4 Hz, 2P), 57.94 (ddd, J = 238.4, 39.2, 21.9 Hz, 1P), −143.55 (hept, J = 711.5 Hz, PF_6^-). ^{19}F{^{1}H}-NMR (373 MHz, DMSO-d_6) δ −163.03 (s), −70.03 (d, J = 717.3 Hz, PF_6^-).

Determination of the distribution coefficient

The distribution coefficient ($\log P_{o/w}$) was determined using the traditional shake-flask method using an octanol–water mixture.[25] The compounds **5-FU**, **Ru-DPPE-Cl** and **Ru-DPPE-5FU** (1 mg each) were first solubilized in 100 μL of DMSO and then diluted in a mixture of equal volumes of water (1000 μL) and *n*-octanol (1000 μL) and shaken continuously (300 rpm) at 37 °C for 6 h on a shaker. The tubes were then centrifuged, and the aliquots of octanol and water layers were pipetted out separately. The absorbances of the respective layers were measured, with necessary dilutions using UV-Vis spectroscopy. Each set of measurements was performed in triplicate. The concentration of the species in each layer was determined from their respective molar extinction coefficient (ε) values, and the corresponding distribution coefficient ($\log P_{o/w}$) was calculated.

DPPH radical scavenging assay

The antioxidant activity of Ru(II)-dppe complexes and the **5-FU** ligand were evaluated using a DPPH radical scavenging assay originally reported by Blois with minor modification.[31] A stock solution of DPPH was prepared by dissolving DPPH (0.010 g, 0.025 mmol) in 100 mL of ethanol, resulting in a dark purple solution (0.25 mM). Stock solutions (1 mM) of **Ru-DPPE-5FU** were prepared in ethanol to be tested, while the stock solutions (1 mM) for **5-FU** and **Ru-DPPE-Cl** were made by first dissolving in 0.5 mL DMSO and diluting with ethanol. The stock solutions were serially diluted in Eppendorf microtubes (2 mL) with ethanol to give 5 samples, each of which had a final volume of 600 μL. Subsequently, 400 μL of DPPH stock solution was added to each sample. The solutions were tested with 0.10 mM DPPH solution in 1 mL of ethanolic solution in the respective concentration ranges. The concentration of **5-FU** varied from 0 to 0.05 mM (0–0.5 equiv.) in 0.01 mM increments, whereas the concentrations of **Ru-DPPE-Cl** and **Ru-DPPE-5FU** varied from 0 to 0.01 mM (0–0.1 equiv.) in 0.002 mM increments. The resulting mixtures were shaken vigorously and stored in the dark at 25 °C for 30 minutes. Thereafter, the absorbance at 517 nm was measured against an ethanol blank using the UV-Vis spectrophotometer to determine the level of discoloration of each sample. EC_{50} values were then determined by fitting the linear region of the data and determining the concentration that gave 50% scavenging activity (EC_{50}).

Theoretical studies

The molecular geometries of **5-FU**, **Ru-DPPE-Cl**, and **Ru-DPPE-5FU**, were optimized by density functional theory calculations at the B3LYP level with the SDD basis set for the Ru metal centre and the 6-31G** basis set for all other atoms using the Gaussian 09 program.[34] The geometry of complex **Ru-DPPE-5FU** was fully optimized from its X-ray crystal structure. Time-dependent density functional theory (TD-DFT) calculations were performed using the same basis set with DCM as the solvent. TD-DFT was used to calculate the 75 lowest energy electronic transition states. The atomic coordinates of all the calculated species are provided in Table S6, ESI.†

Cell culture

The impact of **Ru-DPPE-5FU** treatment on cellular proliferation, migration, and apoptosis were investigated using the human GBM cell line (LN229), which was procured from the cell repository of the National Center for Cell Science (NCCS) Pune, India. Human keratinocyte cell line (HaCaT) was a kind gift from Dr. Manoj Menon (KSBS, IIT Delhi). It was used as a control cell line to measure the S.I. of **Ru-DPPE-5FU**. LN229 cells were cultured in DMEM medium (GIBCO), whereas HaCaT cells were cultured in DMEM-F12 media (GIBCO). Both media were supplemented with 10% fetal bovine serum (FBS), penicillin (100 U mL^{-1}) and streptomycin solution (100 μg mL^{-1}). Cell lines were maintained in a humidified atmosphere having 5% CO_2 at 37 °C. The cells were regularly passaged upon reaching 75–80% confluency.

Determination of the IC_{50} value

The half maximum inhibitory concentrations (IC_{50}) of **5-FU**, **Ru-DPPE-Cl**, and **Ru-DPPE-5FU** were determined by performing the MTT cell viability assay as described previously.[16] Briefly, about 10×10^3 LN229 GBM cells were seeded in triplicate in each well of a 96-well plate. The next day, the cells were treated with various concentrations of the tested compounds dissolved in cell culture medium. It was ensured that the final concentration of DMSO solvent did not exceed 0.4%. After incubating the cells for 24 h with the drugs, the spent medium was carefully aspirated and replaced with fresh medium containing 0.5 mg mL^{-1} of (3-(4,5-di-methylthiazole-2-yl)-2,5-diphenyl tetrazolium bromide) MTT reagent. The plate was incubated for 2 h in the dark, following which the MTT solution was removed, and the formazan crystals generated were dissolved in 100 μL of DMSO solution. The absorbance was measured at 595 nm using a microplate reader. The cell viability was calculated by using the following formula:

$$\%\,\text{Cell viability} = \frac{\text{absorbance (treated)} - \text{absorbance (blank)}}{\text{absorbance (untreated)} - \text{absorbance (blank)}} \times 100 \quad (1)$$

The IC_{50} values of the drugs were calculated using the GraphPad Prism® software by plotting the % cell viability against the drug concentration. The experiment was conducted

three times (n = 3), and each data point was collected in triplicate.

The selectivity index (S.I.) for **Ru-DPPE-5FU** was measured using the HaCaT cell line as the control/normal cells. The selectivity index (S.I.) of the drug was calculated using the following formula:

$$\text{S.I.} = \frac{\text{Normal cell line (HaCaT) IC}_{50}}{\text{GBM cell line (LN229) IC}_{50}} \quad (2)$$

In general, the drugs with S.I. ≥ 3 show more selectivity towards cancerous cells.[16]

MTT-based cell proliferation assay

The effect of **Ru-DPPE-5FU** as a lead compound on cellular proliferation was investigated by performing an MTT-based cell viability assay. About 5×10^5 cells were seeded in each well of a 96-well plate in triplicate. The next day, the cells were treated with fresh medium (untreated control) or **Ru-DPPE-5FU** (at a concentration of 1 μM)-containing medium. The viability of the treated and untreated cells was measured at designated time points according to the above-mentioned protocol. The relative cellular proliferation was calculated by plotting the fold change in cell viability as compared to day 0.

3D spheroid formation assay

The ability of GBM cells to generate three-dimensional (3D) spheroids in the presence and absence of **Ru-DPPE-5FU** was evaluated by performing the 3D spheroid formation assay. Briefly, each well of a 96-well plate was coated with 1% agarose solution (in PBS), which gave a U-shape at the bottom and prevented the cells from adhering to the substratum. About 10×10^3 LN229 cells dissolved in 100 μL of medium (with or without **Ru-DPPE-5FU**) were added to each well. The cells were allowed to come together and form spheroids for the next 4–5 days. Finally, the spheroids were imaged with an inverted microscope when the diameters of the control spheroids reached a minimum of 400 μm.

In vitro scratch assay

The effect of **Ru-DPPE-5FU** treatment upon cellular migration was studied by performing the scratch assay or wound healing assay. Briefly, about 1×10^5 LN229 cells were seeded in each well of a 12-well plate. The next day, the cells were treated with fresh medium or medium containing **Ru-DPPE-5FU** at a final concentration of 1 μM. The cells were incubated for 48 h in the presence/absence of the drug. Subsequently, straight lines were scratched on the monolayer of cells using sterile 200 μL pipette tips, and detached cells were washed off using PBS. The cells were maintained in a serum-free medium for the next 24 h and the relative migration of the cells was monitored between the control and treated cells for wound closure. Relative migration was calculated using the following formula:

$$\text{Relative migration} = \frac{\text{scratch distance } (t = 0\text{ h}) - \text{scratch distance } (t = 24\text{ h})}{\text{scratch distance } (t = 0\text{ h})} \quad (3)$$

Caspase 3/7 assay

The effect on programmed cell death or apoptosis was investigated by measuring the activity of two major executioner caspases, namely, caspase 3 and 7. Approximately 1×10^5 LN229 cells were seeded in each well of a 12-well plate. The following day, the cells were treated with fresh medium or **Ru-DPPE-5FU** (at 1 μM concentration) for 48 h. After treatment, 5000 cells from both the control and treated groups were collected. The caspase activity between both cell groups was checked after the addition of Caspase-Glo 3/7 reagent as per the manufacturer's protocol (Promega, USA). Briefly, cells were gently mixed with caspase reagent and incubated at room temperature for 1.5 h. Later, the caspase activity based on luminescence was measured using a luminometer (Berthold, Germany). Three independent experiments were performed to measure the relative caspase activity.

AO/EB dual staining

The acridine orange/ethidium bromide (AO/EB) dual staining method was used to identify apoptotic cells in the control and **Ru-DPPE-5FU**-treated LN229 cells. About 1×10^5 cells were seeded in each well of a 12-well plate and were allowed to attach overnight. The next day, the spent medium was replaced with fresh DMEM (untreated control) and the **Ru-DPPE-5FU**-containing medium (at a concentration of 1 μM). After 24 h incubation with the drug, the medium was removed, washed with PBS, and the cells were incubated with a dual AO/EB staining solution (50 μg mL^{-1} each dye) for 5 min. Finally, the dye-containing medium was removed, and the cells were washed with warm PBS before imaging with a fluorescence microscope.

For the AO/EB dual staining of 3D spheroids, a similar protocol was followed. The spheroids of untreated LN229 cells were allowed to form as discussed above. When the diameter of the spheroids reached about 300 μm, the medium in each well was very carefully removed and replaced with fresh DMEM or medium containing 1 μM **Ru-DPPE-5FU**. After two days of incubation, the spheroids were washed and stained with dual AO/EB staining solution as mentioned above. Apoptotic cells were identified by their nuclear condensation and blebbing.

Author contributions

A. S., R. M. and A. K. P.: Conceptualization, design of research problem and studies. A. S.: Synthesis, methodology, characterizations, execution of experiments, validation, formal analysis, writing-original draft of the manuscript. I. M., A. K., and R. K.: Design, execution, analysis, writing drafts biological experiments; here I. M., and A. K. contributed equally to the manuscript. A. K. S.: theoretical calculations like DFT, ESP

plots *etc.* A. K. P., R. K.: supervision, project administration, funding acquisition, manuscript writing and editing. All the authors discussed to the results and finalized the manuscript.

Conflicts of interest

The authors declare no competing financial interest.

Acknowledgements

A. S. is grateful to Ministry of Human Resource and Development (MHRD) for the fellowship, R. M. thanks the Council of Scientific and Industrial Research (CSIR), A. K. P. acknowledge Council of Scientific and Industrial Research (CSIR) for financial support (No. 01(3048)/21/EMR-II) and Indian Council of Medical Research (ICMR) (Project No. 2020-2677), R. K. thanks the Science and Engineering Research Board (SERB), Government of India for the financial support (CRG/2020/004640). I. M. is thankful to Ministry of Human Resource and Development (MHRD), Govt. of India for the award of Senior Research Fellowship. A. K. acknowledges the Department of Biotechnology (DBT), Govt. of India for the award of Junior Research Fellowship (DBT/2020/IIT-D/1484), and A. S. is thankful to Dr Sharad K. Sachan, Dept. of Chemistry, IITK for the suggestions in crystal structure analysis, and we also acknowledged Computer Centre IIT Kanpur for providing High Performance Computing (HPC-2013) facility for the DFT calculations.

References

1 R. G. Kenny and C. J. Marmion, *Chem. Rev.*, 2019, **119**, 1058–1137.
2 Z. Guo and P. J. Sadler, *Angew. Chem., Int. Ed.*, 1999, **11**, 1512–1531.
3 K. D. Mjos and C. Orvig, *Chem. Rev.*, 2014, **114**, 4540–4456.
4 C. S. Allardyce and P. J. Dyson, *Dalton Trans.*, 2016, **45**, 3201–3209.
5 E. Alessio, *Eur. J. Inorg. Chem.*, 2017, **12**, 1549–1560.
6 S. Thota, D. A. Rodrigues, D. B. Crans and E. J. Barreiro, *J. Med. Chem.*, 2018, **61**, 5805–5821.
7 F. E. Poynton, S. A. Bright, S. Blasco, D. C. Williams, J. M. Kelly and T. Gunnlaugsson, *Chem. Soc. Rev.*, 2017, **46**, 7706–7756.
8 C. Mari, V. Pierroz, S. Ferrari and G. Gasser, *Chem. Sci.*, 2015, **6**, 2660–2686.
9 R. Trondl, P. Heffeter, C. R. Kowol, M. A. Jakupec, W. Berger and B. K. Keppler, *Chem. Sci.*, 2014, **5**, 2925–2932.
10 R. Y. Bai, V. Staedtke and G. J. Riggins, *Trends Mol. Med.*, 2011, **17**, 301–312.
11 R. Stupp, W. P. Mason, M. J. Van Den Bent, M. Weller, B. Fisher, M. J. B. Taphoorn, K. Belanger, A. A. Brandes, C. Marosi, U. Bogdahn, J. Curschmann, R. C. Janzer, S. K. Ludwin, T. Gorlia, A. Allgeier, D. Lacombe, J. G. Cairncross, E. Eisenhauer and R. O. Mirimanoff, *N. Engl. J. Med.*, 2005, **352**, 987–996.
12 (*a*) J. Chen, R. M. McKay and L. F. Parada, *Cell*, 2012, **149**, 36–47; (*b*) S. C. Li, L. T. Vu, H. W. Ho, H. Z. Yin, V. Keschrumrus, Q. Lu, J. Wang, H. Zhang, Z. Ma, A. Stover, J. H. Weiss, P. H. Schwartz and W. G. Loudon, *Cancer Cell Int.*, 2012, **12**, 41.
13 J. Polivka Jr., J. Polivka, L. Holubec, T. Kubikova, V. Priban, O. Hes, K. Pivovarcikova and I. Treskova, *Anticancer Res.*, 2017, **37**, 21–34.
14 M. Wang, X. Jiang, F. Wu, H. Xu, Z. Lin, B. Qi and H. Xia, *Glioma*, 2018, **1**, 79–88.
15 S. Saha, V. Yakati, G. Shankar, M. M. C. S. Jaggarapu, G. Moku, K. Madhusudana, R. Banerjee, S. Ramkrishna, R. Srinivas and A. Chaudhuri, *J. Mater. Chem. B*, 2020, **8**, 4318–4330.
16 P. Kumar, I. Mondal, R. Kulshrestha and A. K. Patra, *Dalton Trans.*, 2020, **49**, 13294–13310.
17 S. Lakkadwala and J. Singh, *J. Pharm. Sci.*, 2018, **107**, 2902–2913.
18 K. G. Liu, X. Q. Cai, X. C. Li, D. A. Qin and M. L. Hu, *Inorg. Chim. Acta*, 2012, **388**, 78–83.
19 Z. J. Li, Y. Hou, D. A. Qin, Z. M. Jin and M. L. Hu, *PLoS One*, 2015, **10**, e0120221.
20 V. R. Silva, R. S. Correa, L. de S. Santos, M. Botelho, P. Soares, A. A. Batista and D. P. Bezerra, *Sci. Rep.*, 2018, **8**, 288.
21 B. P. Sullivan and T. J. Meyer, *Inorg. Chem.*, 1982, **21**, 1037–1040.
22 M. M. da Silva, G. H. Ribeiro, M. S. de Camargo, A. G. Ferreira, L. Ribeiro, M. I. F. Barbosa, V. M. Deflon, S. Castelli, A. Desideri, R. S. Correa, A. B. Ribeiro, H. D. Nicolella, S. D. Ozelin, D. C. Tavares and A. A. Batista, *Inorg. Chem.*, 2021, **60**, 14174–14189.
23 L. Fallon III, *Acta Crystallogr., Sect. B: Struct. Crystallogr. Cryst. Chem.*, 1973, **29**, 2549–2556.
24 G. H. Ribeiro, A. P. M. Guedes, T. D. de Oliveira, C. R. S. T. b. de Correia, L. Colina-Vegas, M. A. Lima, J. A. Nobrega, M. R. Cominetti, F. V. Rocha, A. G. Ferreira, E. E. Castellano, F. R. Teixeira and A. A. Batista, *Inorg. Chem.*, 2020, **59**, 15004–15018.
25 E. Baka, J. E. A. Comer and K. Takacs-Novak, *J. Pharm. Biomed. Anal.*, 2008, **46**, 335–341.
26 L. M. Sayre, G. Perry and M. A. Smith, *Chem. Res. Toxicol.*, 2008, **21**, 172–188.
27 A. T. Y. Lau, Y. Wang and J.-F. Chiu, *J. Cell. Biochem.*, 2008, **104**, 657–667.
28 P. Srivastava, R. Mishra, M. Verma, S. Sivakumar and A. K. Patra, *Polyhedron*, 2019, **172**, 132–140.
29 M. Valko, D. Leibfritz, J. Moncol, M. T. D. Cronin, M. Mazur and J. Telser, *Int. J. Biochem. Cell Biol.*, 2007, **39**, 44–84.
30 C. Gorrini, I. S. Harris and T. W. Mak, *Nat. Rev. Drug Discovery*, 2013, **12**, 931–947.
31 M. S. Blois, *Nature*, 1958, **181**, 1199–1200.
32 M. C. Foti, *J. Agric. Food Chem.*, 2015, **63**, 8765–8776.

33 C. Mu, K. E. Prosser, S. Harrypersad, G. A. MacNeil, R. Panchmatia, J. R. Thompson, S. Sinha, J. J. Warren and C. J. Walsby, *Inorg. Chem.*, 2018, **57**, 15247–15261.
34 M. J. Frisch, G. W. Trucks, H. B. Schlegel, G. E. Scuseria, M. A. Robb, J. R. Cheeseman, G. Scalmani, V. Barone, G. A. Petersson, H. Nakatsuji, X. Li, M. Caricato, A. Marenich, J. Bloino, B. G. Janesko, R. Gomperts, B. Mennucci, H. P. Hratchian, J. V. Ortiz, A. F. Izmaylov, J. L. Sonnenberg, D. Williams-Young, F. Ding, F. Lipparini, F. Egidi, J. Goings, B. Peng, A. Petrone, T. Henderson, D. Ranasinghe, V. G. Zakrzewski, J. Gao, N. Rega, G. Zheng, W. Liang, M. Hada, M. Ehara, K. Toyota, R. Fukuda, J. Hasegawa, M. Ishida, T. Nakajima, Y. Honda, O. Kitao, H. Nakai, T. Vreven, K. Throssell, J. A. Montgomery Jr., J. E. Peralta, F. Ogliaro, M. Bearpark, J. J. Heyd, E. Brothers, K. N. Kudin, V. N. Staroverov, T. Keith, R. Kobayashi, J. Normand, K. Raghavachari, A. Rendell, J. C. Burant, S. S. Iyengar, J. Tomasi, M. Cossi, J. M. Millam, M. Klene, C. Adamo, R. Cammi, J. W. Ochterski, R. L. Martin, K. Morokuma, O. Farkas, J. B. Foresman and D. J. Fox, Gaussian, Inc., Wallingford, CT, 2010.
35 D. Andrae, U. Häußermann, M. Dolg, H. Stoll and H. Preuß, *Theor. Chim. Acta*, 1990, **77**(2), 123–141.
36 A. Vlček Jr. and S. Záliš, *Coord. Chem. Rev.*, 2007, **251**, 258–287.
37 S. Karmakar, D. Maity, S. Mardanya and S. Baitalik, *Dalton Trans.*, 2015, **44**, 18607–18623.
38 *APEX2 v2012.4*, Bruker AXS, Madison, WI, 1999.
39 N. Walker and D. Stuart, *Acta Crystallogr., Sect. A: Fundam. Crystallogr.*, 1983, **39**, 158–166.
40 *SMART & SAINT Software Reference manuals, Version 6.45*, Bruker Analytical X-ray Systems, Inc., Madison, WI, 2003.
41 G. M. Sheldrick, *SADABS, Area Detector Absorption Correction*, University of Göttingen, Göttingen, Germany, 2001.
42 (*a*) G. M. Sheldrick, *Acta Crystallogr., Sect. A: Fundam. Crystallogr.*, 2008, **64**, 112–122; (*b*) G. M. Sheldrick, *SHELXTL 6.14*, Bruker, AXS Inc., Madison, WI, 2000.
43 O. V. Dolomanov, L. J. Bourhis, R. J. Gildea, J. A. K. Howard and H. Puschmann, OLEX2: a complete structure solution, refinement and analysis program, *J. Appl. Crystallogr.*, 2009, **42**, 339–341.
44 M. T. Bautista, E. P. Cappellani, S. D. Drouin, R. H. Morris, C. T. Schweitzer, A. Sella and J. Zubkowski, *J. Am. Chem. Soc.*, 1991, **113**, 4876–4887.